

Copyright
by
Marcia Joyce Isakson
2002

The Dissertation Committee for Marcia Joyce Isakson
Certifies that this is the approved version of the following dissertation:

**The Effects of Alignment on the Dissociation of H₂
on Pd(111)**

Committee:

Greg O. Sitz, Supervisor

Alan Campion

Michael Downer

Manfred Fink

Charles Mullins

**The Effects of Alignment on the Dissociation of H₂
on Pd(111)**

by

Marcia Joyce Isakson, B.S.,M.A.

DISSERTATION

Presented to the Faculty of the Graduate School of
The University of Texas at Austin
in Partial Fulfillment
of the Requirements
for the Degree of

DOCTOR OF PHILOSOPHY

THE UNIVERSITY OF TEXAS AT AUSTIN

May 2002

Dedicated to my husband, John M. Isakson, who supported me with all
his heart.

Acknowledgments

My time in graduate school and the completion of this project was a tremendously rewarding and challenging experience. I would like to thank the people who made it possible. First and foremost, I would like to thank my advisor, Dr. Greg Sitz, who helped me to discover how interesting surface science can be. He truly demonstrated what it is to be a great scientist and teacher. I would also like to thank all of the other students without whom this project would have never happened. These other scientists not only made my job easier, they made it much more fun. In particular, I would like to thank Leah Schackman, with whom I enjoyed many lively and helpful conversations and who helped me keep the laser alive, Dr. Jenny Siders, who will be a friend for life, and Dr. Elizabeth Watts, who taught me the nuances of two laser experimentation. I also enjoyed the company of many other students in my time in this lab which spanned ten years: Jerry Kim who is now experimenting in the chamber which I began building almost nine years ago, Michael Gostein, who did preliminary alignment measurements, Michelle Gotthold, Todd Tinsley, David Schlichte, Peter Bach and James Ayers. Lastly, I would like thank my committee members, Manfred Fink, Buddy Mullins, Alan Campion and Michael Downer for their time and insight.

The Effects of Alignment on the Dissociation of H₂ on Pd(111)

Publication No. _____

Marcia Joyce Isakson, Ph.D.
The University of Texas at Austin, 2002

Supervisor: Greg O. Sitz

The effects of rotational alignment in surface scattering phenomena are studied. Alignment means a spatial preference for the plane of rotation. Specifically, changes in the reflection probability for H₂ reaction with Pd(111) were studied for different molecular rotational alignments (helicopters vs. cartwheelers) and different incident translational energies. Experimentally, molecules were prepared with well-defined, non-statistical alignments using a linearly polarized laser before interaction with the surface. After scattering, the molecules were probed with another laser to determine their internal state. We found that the reflectivity of helicopter molecules was less than that of cartwheeler molecules. This effect increased with increasing incident energy. The result is interpreted as meaning that helicopters are more likely to dissociate than to scatter. The results are further evidence of steric forces in the H₂/Pd interaction.

Table of Contents

Acknowledgments	v
Abstract	vi
List of Tables	ix
List of Figures	x
Chapter 1. Introduction	1
1.1 The Theory of Gas-Surface Scattering Dynamics	4
1.1.1 Calculating the Potential Energy Surface	5
1.1.2 Simulating the Dynamics	7
1.1.3 Dissociative Adsorption	9
1.2 Relevant Simulations and Experiments	10
1.2.1 The Theory of Steric Effects	10
1.2.2 Prediction of Alignment Effects	14
1.2.3 Previous Alignment Experiments	17
Chapter 2. Experimental Set-Up	21
2.1 Apparatus	21
2.2 State Preparation	23
2.3 Detection of Molecules	24
2.4 The Pd(111) Surface	25
2.4.1 Geometry	25
2.4.2 Surface Preparation	26
Chapter 3. Spectroscopy	28
3.1 The Line Strength Equation	28
3.1.1 The Basic Equation	28
3.1.2 The Experimental Sensitivity Factor, $C(det)$	30
3.1.3 The Moments of the Ground State Distribution, $A_q^{(k)}(J_i)$	30
3.1.4 The Population of the Ground State, $n(J_i)$	31

3.1.5	The Moments of the Line Strength, P_q^k	31
3.2	Making an Aligned Distribution: Stimulated Raman Scattering	40
3.3	Detecting molecules through a two-photon REMPI Process	43
Chapter 4.	Results and Conclusions	47
4.1	Characterization of the Aligned States	47
4.2	Survival Probabilities of Aligned States	53
4.3	The Stark Effect	58
4.4	Discussion	60
Chapter 5.	Future Work	63
5.1	Extending the Energy Range of the Alignment Experiment	63
5.2	Alignment Effects in Other Ro-vibrational States	64
5.3	Inelastic Scattering Experiments Using the J=3 Temporally Isolated Signal	65
5.4	Measurement of the Time Development of the Hyperfine Depolarization Factor for H ₂	67
Appendix		68
Appendix A.	Alignment How-To's	69
Bibliography		75
Vita		80

List of Tables

3.1	Nomenclature for the two-photon line strength equation. These are defined as in reference [1].	29
4.1	Sticking Coefficients and Inelastic Scattering Probabilities for $J=3$. The transition probability for $J = 3 \rightarrow 5$ value is calculated from the apparent activation energy found in reference [2].	61

List of Figures

1.1	Coordinate system used for simulations and experiments of the dissociation of diatomics on metals. In the figure, x, y , and z are the center of mass coordinates, r is the bond length of the molecule, θ is the polar angle of the molecule with the surface normal and ϕ is the azimuthal angle. This figure was taken from reference [3].	3
1.2	A graphical description of alignment in the classical sense. Molecules with J vectors aligned perpendicular to the surface normal are known as cartwheelers. Those with J vectors aligned parallel to the surface normal are helicopters. .	4
1.3	Aligned distributions can be produced quantum mechanically by having an unequal distribution of the population among m_J states. This distribution describes a cartwheel state if the quantization axis is taken as a vector perpendicular to the surface normal. Typically the quantization axis is taken as the electric field of the laser when describing the state preparation process.	5
1.4	Contour plots of the PES for the $H_2/Pd(100)$ system, from references [4],[5], and [6]. The plots keep all degrees of freedom except the distance to the surface, z , and the bond length, r , constant. The inset shows the dissociation of the molecule graphically.	11
1.5	Sticking coefficient of H_2 on $Pd(111)$ as a function of incident energy. The squares are the rotationally averaged sticking coefficient measured by Gostein and Sitz [7]. The circles were reported by Beutl et al [8]. Note that the both find the lowest sticking coefficients from 50-75 meV. Here the steric mechanism is not yet applicable and the molecules do not have enough translational energy to overcome the barriers directly.	13
1.6	A highly anisotropic PES for the H_2/Pd system constructed by Busnengo. Molecules will be steered into favorable (helicopter) alignments by this type of PES. From Reference [9].	15
1.7	Sticking probability versus initial rotational state for different alignment distributions in the $H_2/Pd(100)$ system. The initial kinetic energy was 190 meV. Note how there is a preference for sticking for helicopter distributions. From Reference [10].	16

2.8	Computed reaction probabilities for the H ₂ /Cu(100) system. Note that alignment enhancement is much more pronounced at high translational energies. Here high m_J states are helicopter molecules and low m_J states are cartwheelers. From Reference [11].	16
2.1	Experimental Set-up.	22
2.2	Three dimensional picture of the experimental set-up.	22
2.3	The timing of the pumped molecular pulse versus the thermal background pulse. Note how the pumped molecules are easily distinguishable from the thermal background due to the vast difference in time scales. The signal from the pumped molecules was often ten times greater than that of the thermal background.	24
2.4	Diagram of the surface geometry of the Pd(111) surface. The surface is highly isotropic and flat.	26
3.1	A geometric interpretation of angular momentum coupling. In the figure $\vec{J} = \vec{J}_1 + \vec{J}_2$ and $m = m_1 + m_2$. Because of the precession of \vec{J}_1 and \vec{J}_2 about \vec{J} , m_1 and m_2 are not constants of the motion.	34
3.2	A geometric interpretation of angular momentum coupling in hyperfine depolarization. In the figure $\vec{F} = \vec{J} + \vec{I}$ and $m_F = m_J + m_I$. Because of the precession of \vec{J} and \vec{I} about \vec{F} , m_J and m_I are not constants of the motion. For odd J states of H ₂ , there are two additional spin states, \vec{I} that couple with \vec{J} . For even J states, I = 0 and there is no depolarization.	36
3.3	The hyperfine depolarization factor for H ₂ . Shown are calculated values for P ₀ ⁰ (solid line), P ₀ ² , (dashed line), and P ₀ ⁴ , (triangles). Note how hyperfine depolarization is less of a factor as J increases. Note also how even J's are not depolarized because I=0.	37
3.4	Allowed two photon transitions for $\Sigma \rightarrow \Sigma$ transitions. This figure was adapted from reference [12].	39
3.5	Creating an aligned distribution through an S branch transition. Molecules begin in an isotropic J=1 state with equal population in $m = 0, \pm 1$. As molecules are pumped to J=3 $\Delta m = 0$ so only the central m_J states are populated creating an aligned distribution. Molecules in J=3 with equal population is $m_J = 0, \pm 1$ and no population in the other m-states would have a quadrupole moment of -0.73.	42

3.6	Two photon transitions involved in preparing and detecting aligned molecules in H ₂ . The detection of the molecules proceeds via the 2+1 REMPI process. The rotational states in the E,F ¹ Σ _g ⁺ electronic state was J=3 for the Q branch measurements and J=5 for the S branch measurements. . .	44
3.7	Calculated ion intensity for the quadrupole moment of the linestrength factor normalized by the population, P ₀ ² /P ₀ ⁰ . Here θ corresponds to the polarization of probe laser relative to the pump laser. Note the intensity changes much more for the S branch.	45
3.8	Signal strength of S vs Q branches for H ₂ . The laser power at the frequency of the S branch transitions is about half of that for the Q branch transitions. The line strength for the S branch is about 10% of the Q branch line strength. .	46
4.1	The calculated relative moments of the line strength for different values of J for the S branch in the E,F ¹ Σ _g ⁺ ← X ¹ Σ _g ⁺ transition in H ₂	49
4.2	Change in ion intensity for the S(3) branch due to a change in the relative polarizations of the pump and probe lasers. In this configuration, the pump laser is polarized parallel to the surface normal.	50
4.3	The classical representation of the angles the J vector makes with the quantization axis for different m-states.	51
4.4	Time dependence of the quadrupole moment of HF due to hyperfine depolarization for J=3 and J=10 due to the evolution of $\vec{J} \cdot \vec{I}$. As the magnitude of J increases there is less effect. Note that in the time range of our experiment there is considerable oscillatory behavior. Taken from reference [13].	52
4.5	Change in ion intensity for the S(3) branch due to a change in the relative polarizations of the pump and probe lasers. In this configuration, the pump laser is polarized perpendicular to the surface normal.	53
4.6	Time of flight measurement from a cold (~ 100K H ₂ covered surface. The reflectivity for this type of measurement was found to be between 0.97 and 1.0 when summed over a range of scattering angles. The incident energy of this measurement was 68 meV.	54
4.7	Incident and scattered beam profiles of the two distributions corresponding to different polarizations of the pump laser. In the figure, the horizontally polarized incident distribution is given by ●, the vertically polarized incident distribution is given by ○, the horizontally polarized scattered distribution is given by ■, and the vertically polarized scattered distribution is given by □.	56

4.8	Time of flight measurement for two different polarizations of the pump laser. The horizontal polarization (■) will create a distribution that has a preference for the cartwheeler motion. The vertical polarization distribution (○) contains both helicopters and cartwheelers. The incident energy for this measurement was 64 meV. The calculated normalized ratio of the horizontal polarization distribution's scattered signal to that of the vertical polarization was 1.53.	57
4.9	The ratio of the scattered signal from the horizontal polarization of the pump laser to that of the vertically polarized pump laser for different incident energies. Note that the ratio is highest at the energy where the steric mechanism is balanced by the ability of the molecule to overcome the barrier with incident translational energy.	58
4.10	Simulated profile of the $B^1\Sigma_u^+ \leftarrow X^1\Sigma_g^+$ transition of spatially isotropic H_2 . In the simulation the maximum intensity of the Gaussian beam profile was 10 GW/cm^2 with a linewidth of $\Delta\nu = 1.0 \text{ cm}^{-1}$. The contribution of each m_J state is shown in thin lines. This figure is taken from reference [38].	59
4.11	Measured linewidth at various laser intensities. The highest intensity is given by □, 60% laser intensity is given by ○, and 25% laser intensity is given by ■ filled squares. Note how the line profile does not change with laser intensity. Each line profile can be fit with a Gaussian.	60
5.1	TOF measurement of $J=5$ (□) and $J=3$ (●). Note that there is some pumping into $J=5$ as evidenced by the temporally isolated $J=5$ signal that is coincident with the incident $J=3$. It is difficult to discern any $J=5$ scattering. This data was taken at an incident energy of 54 meV.	66

Chapter 1

Introduction

The physics of reactions at surfaces is an interesting and relevant field. Surfaces often act as catalysts by providing reaction sites for gaseous species. In the automobile industry, catalysts are used to convert noxious CO into CO₂ in the exhaust system. Catalysts are used in the chemical industry to synthesize ammonia and methanol. In the atmosphere, ice particles in clouds act as catalysts for an important step in the destruction of the ozone layer. As industry becomes more and more sophisticated, designer catalysts become more and more desirable. However, although one can imagine a multitude of combinations of the elements to make a catalyst, testing each one in the lab is unrealistic. Therefore, modelling catalysts has become a burgeoning field.

Catalytic reactions are intrinsically complicated. For example, in the reaction that takes place in the destruction of the ozone layer, two species must be adsorbed, dissociated, diffuse across the surface, react and then the reactant must desorb. While on the surface, reactants can diffuse across or into the surface, or desorb before reacting. In most catalytic reactions the rate limiting step is the adsorption and dissociation of the reacting species. Therefore, a fundamental description of the adsorption and dissociation of molecular species on surfaces is critically important to the understanding of the entire catalytic reaction.

Theorists, beginning with Lennard-Jones in 1932 [14], have struggled to understand the basics of how molecules scatter from and dissociate on surfaces. The problem is inherently complex because it involves many degrees of freedom of the molecule and the surface. A diatomic molecule approaching a surface has six degrees of freedom. These are generally identified in the following manner. (See figure 1.1.) The letters x and y identify where the molecule is above the surface as a 2D plane. This is important in identifying whether the molecule is approaching over a bridge site, on top of a surface atom or varying other places depending on the symmetry of the surface. The letter, z , is taken as the distance from the center of mass of the molecule to the surface. The letter r denotes the bond length of the molecule. It can be time dependent if the molecule is vibrating. Finally the Greek letters, θ and ϕ , denote the angle between the molecular bond and the surface normal and the azimuthal angle, respectively. In a rotating molecule these are time dependent. This work is primarily concerned with the dependence of surface processes on the angle, θ . Specifically, we will look at the role that the alignment of the incident molecule has in molecular scattering and dissociation in the $\text{H}_2/\text{Pd}(111)$ system.

Since this work is concerned with molecular alignment, let us first discuss alignment conventions. Consider rotational motion classically, molecules with the J vector perpendicular to the surface normal are known as cartwheeler molecules. (See figure 1.2.) As one can see in the figure, there are a range of cartwheeler motions. Molecules with J vectors parallel to the surface normal are known as helicopter molecules. If we wish to consider the molecules quantum mechanically, we can take a vector of

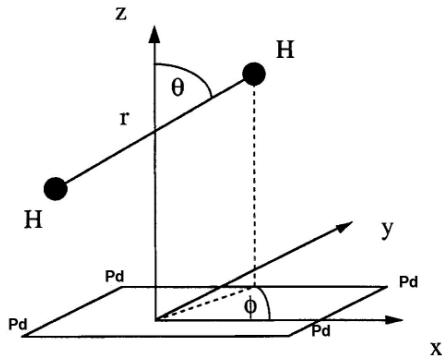


Figure 1.1: Coordinate system used for simulations and experiments of the dissociation of diatomics on metals. In the figure, x, y , and z are the center of mass coordinates, r is the bond length of the molecule, θ is the polar angle of the molecule with the surface normal and ϕ is the azimuthal angle. This figure was taken from reference [3].

our choice to be the quantization axis. (In this type of experiment this vector is conveniently taken as the electric field of the laser. This will be explained in more detail in the experimental section.) We then define alignment in terms of the projection of the rotational vector, J , on a space fixed axis, the quantization axis. This projection is called m_J . If the quantization axis is perpendicular to the surface normal, \hat{n} molecules with low m_J will be helicopters. If we define the quantization axis as along the surface normal then molecules with low m_J are cartwheelers. It should be noted however, that quantum mechanically, there are no true helicopters or cartwheelers since the J vector is not at a well defined position with respect to the surface normal, but is described by a probability distribution labelled by J and m_J . (See Figure 1.3.) Therefore the assignment of helicopter and cartwheeler states are qualitative. The sign of the J vector describes the helicity of the motion (clockwise or counter clockwise). This parameter is called orientation and is not considered in this study.

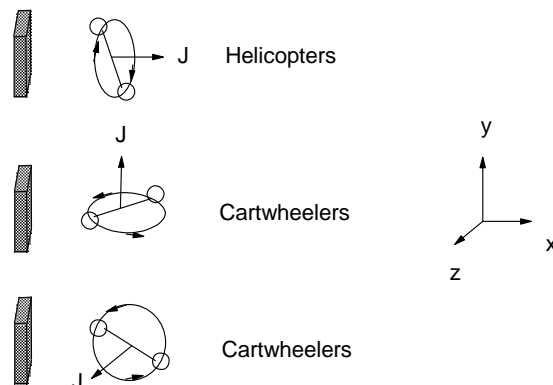


Figure 1.2: A graphical description of alignment in the classical sense. Molecules with J vectors aligned perpendicular to the surface normal are known as cartwheelers. Those with J vectors aligned parallel to the surface normal are helicopters.

It should be noted that orientation has other meanings in the literature beside the helicity of the rotation. For heteronuclear diatomic molecules, such as NO or HCl, orientation often describes which atom is pointed toward the surface in the interaction. There is often a distinctly different PES for the presentation of each atom. Because of this, in the literature, authors often use the term, orientation, to describe alignment.

In this paper, I will review the theory behind the effects of alignment on surface processes, discuss previous alignment experiments, illustrate how the current measurements were obtained and then present and discuss my results.

1.1 The Theory of Gas-Surface Scattering Dynamics

Those who wish to describe the approach of a molecule to a surface generally use the following approach: 1) Construct a potential energy surface (PES) for the molecule as it approaches the surface, 2) Calculate

Quantum Mechanical Alignment

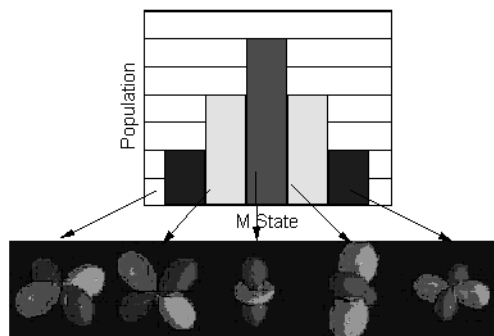


Figure 1.3: Aligned distributions can be produced quantum mechanically by having an unequal distribution of the population among m_J states. This distribution describes a cartwheel state if the quantization axis is taken as a vector perpendicular to the surface normal. Typically the quantization axis is taken as the electric field of the laser when describing the state preparation process.

the dynamics of the molecule as it approaches the surface using either classical or quantum mechanics, and 3) Calculate surface processes such as dissociation for molecules that remain on the surface and calculate scattering dynamics for those that do not. Let us review each step of the process.

1.1.1 Calculating the Potential Energy Surface

Constructing a PES for a particular system, consists of calculating the potential energy for different geometries. For example, a simple one dimensional construct consists of calculating the energy for the molecule based solely on the distance of the molecule from the surface. For atom/atom reactions these types of potential energy curves include the familiar Lennard-Jones model. To construct a higher dimensional PES, one calculates the potential energy in two dimensions and plots the values for the energy as contours. For example one might calculate the

PES for a molecule with a fixed angle θ as the molecule approaches the surface (changing z) and the bond length increases (changing r). A composite 6D PES may be constructed by combining many 2D PES's. The PES's themselves are generally constructed using density functional theory (DFT) with the generalized gradient approximation (GGA). This approach is considered state-of-the-art. For a history of PES construction, a good review is found in a paper by Brivio and Trioni [15].

When calculating the PES for systems involving H_2 and metals, it is assumed that the surface and the molecule do not exchange energy through phonons or electronic transitions. Let us review each assumption. First, in order to squelch energy transfer to and from phonons, the surface is kept at 0 K for the purposes of constructing the PES. This is a huge simplification because the PES does not have to take into account any surface motion or any degrees of freedom of the surface atoms. It is most often thought that the assumption is justified by the large mass difference between the light H_2 molecule and the heavy metal surface atoms. In such a system energy transfer to the surface phonons should be negligible. However, experimental work done by Watts and Sitz in 1998 shows that there is significant energy transfer between scattered molecules and the surface[16]. Watts and Sitz observed a rotational excitation of scattered molecules that had a strong dependence on surface temperature. Therefore the surface and the molecules were definitely exchanging energy and the motion of the molecules (the surface temperature) was having an effect on surface processes. The mechanism is still being debated, but it is clear that the current theory cannot describe this energy exchange well [17]. In defense of a phonon theory, Busnengo et al. developed a theory in which

surface phonons may play a role as the molecule is trapped at the surface long enough for such effects to become important [18]. Therefore, it is not clear what effect the energy exchange with surface phonons may have on surface processes such as dissociation. In this study, the experiment was conducted at a single surface temperature so this parameter was not varied through the course of study.

The second assumption of negligible energy exchange through electronic transitions is justified by the Born-Oppenheimer approximation [4]. In this approximation the electrons are always considered to be in their ground state. In other words, the electron motion follows the nuclear motion adiabatically. This approximation is accurate as long as the atomic velocities are small compared with the electronic velocities. This assumption simplifies the construction of the PES as well because the molecular degrees of freedom are separable from the electronic. Although there are cases when this is not true, all of the theory that is discussed in this work is calculated using this approximation.

If one wishes to calculate the dynamics quantum mechanically, continuous functions of the PES must be used instead of the discrete points produced by DFT. How this is accomplished is highly non-trivial and is described in some detail in a review article by Groß [4].

1.1.2 Simulating the Dynamics

Once the PES is calculated it can be used to simulate the molecular dynamics, that is how the molecule actually behaves as it approaches the surface. Dynamics can be simulated using either a quantum mechanical or a classical description. Let us review the benefits and drawbacks of

each approach.

The classical mechanics approach is much simpler to carry out. The forces on a classically described molecule are calculated for different points on the PES and the molecule moves according to those forces. Simulations are carried out as a series of trajectories where the initial conditions, translational energy, rotational state, etc. are selected at random from the translational, rotational and vibrational temperature distribution being studied. Many trajectories are calculated and the dependence of surface processes on initial conditions is determined statistically. Classical mechanics cannot describe such behavior as tunnelling and zero point energy effects. To describe such behaviors one must calculate the dynamics using quantum mechanics.

A quantum mechanical approach relies on the solution of the Schrödinger equation. In the gas phase, Hamiltonian operator used in the Schrödinger equation depends only on the molecule being studied. As the molecule moves toward the surface and interacts with the surface atoms, the Hamiltonian involves not only the molecule being studied but every surface atom. Even atoms far away from the interaction region have an effect on the motion from mean field theory. Therefore to study the dynamics, we must not only solve the Schrödinger equation for the incident molecule but for the entire surface as well. This process is extremely computationally intensive. Recall also that to describe the motion quantum mechanically, the PES has to be fit to a continuous function, an inexact and error-prone process.

Although much harder to set-up, a quantum mechanical descrip-

tion evolves coherently [4]. In other words, when one simulates quantum mechanically, a plane wave packet probes all impact points simultaneously instead of having to repeat the simulation many times in a statistical fashion to build up a solution as in the classical approach. This is true for angular coordinates as well. Instead of simulating many molecules hitting the surface in a variety of geometries, one may simulate one molecule in a particular (J, m_J) state. Lastly, quantum simulations are needed for slow, light molecules in which the de Broglie wavelength is long rather than fast, heavy molecules. Therefore, for H_2 systems, quantum mechanical calculations are more likely to be needed. I will discuss in detail later, dynamical simulations, both quantum mechanical and classical, which have direct impact on this study.

1.1.3 Dissociative Adsorption

Often the last step in simulating gas-surface interactions is dissociative adsorption. Here a molecule is stretched by the PES so much that the bond breaks and two atoms are adsorbed onto the surface. Consider the PES for the $H_2/Pd(100)$ system calculated by Wilke and Scheffler [5] [6]. (See figure 1.4, part a.) As the molecule approaches the surface it stays close to the path of lowest energy. When the molecule gets sufficiently close to the surface, its bond is stretched until it dissociates. A PES that directs a molecule along such a path is known as an “elbow” plot. Note that along another pathway in plot b of the figure there is a barrier to dissociation. This barrier occurs after the curve or “elbow” in the plot and is known as a “late” barrier. Barriers which occur before the “elbow” are known as “early” barriers and can be overcome with the

molecules incident translational energy. Late barriers can lead to phenomena such as vibrationally enhanced dissociation where the vibrational energy of the molecule allows it to overcome the barrier. Systems which have barriers to dissociation are known as activated systems while those that have no barriers are known as non-activated systems.

As we can see for Pd however, there are some pathways which have barriers and some which do not. Molecules can be directed into non-activated pathways through a process known as steering which I will discuss in the next section.

1.2 Relevant Simulations and Experiments

Now that we understand how molecule simulations are constructed let us review some important predictions of the simulations. I will discuss two predictions in detail, molecular steering and enhanced dissociation for favorable alignment.

1.2.1 The Theory of Steric Effects

In several molecular beam experiments, it has been found that the sticking probability of H₂ molecules initially decreases with increasing incident energy [19] [20]. These findings were contrary to standard theory because translational energy should be used to overcome any early barriers to dissociation and late barriers should be overcome by vibrational energy. One theory used to explain this phenomena was a precursor mechanism. In this theory, the molecule is initially adsorbed in a physisorbed state and then dissociated. Population of the physisorbed state can occur because molecules lose energy to surface phonons [21]. Once the molecule

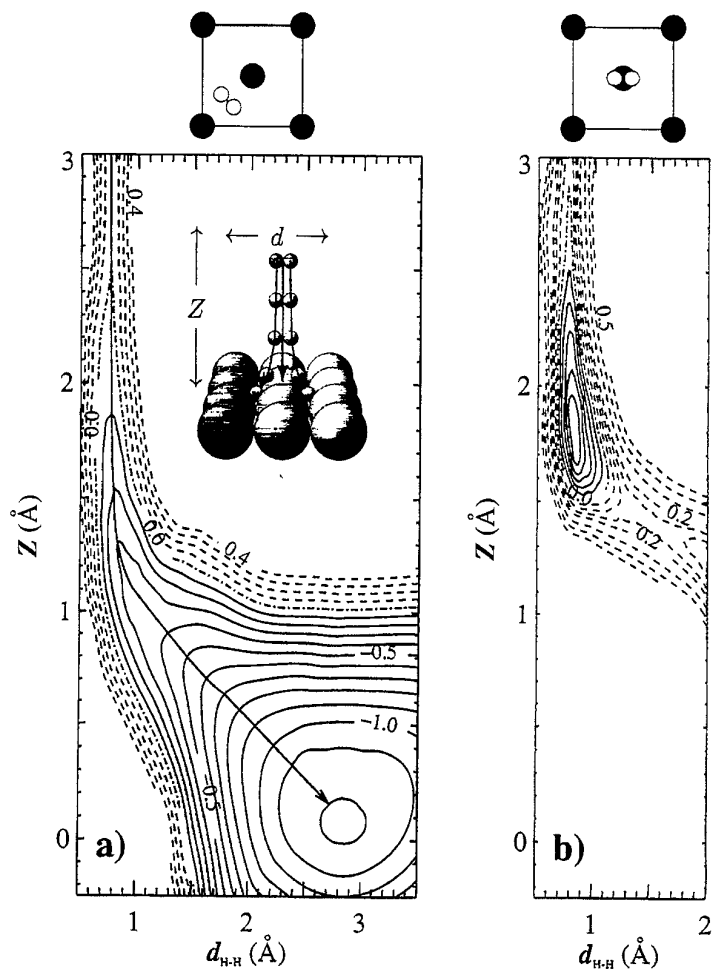


Figure 1.4: Contour plots of the PES for the $\text{H}_2/\text{Pd}(100)$ system, from references [4],[5], and [6]. The plots keep all degrees of freedom except the distance to the surface, z , and the bond length, r , constant. The inset shows the dissociation of the molecule graphically.

is physisorbed to the surface, it can dissociate through different pathways. Molecules with low incident energy are more likely to be physisorbed because the well depth for the molecularly adsorbed state was thought to be relatively shallow. Therefore, molecules with decreased incident energy would be more likely to be trapped in this well and subsequently dissociated.

In 1995, Groß, Wilke and Scheffler reported results from full 6D quantum mechanical simulations that showed that a steric mechanism rather than a precursor mechanism may dominate in the $\text{H}_2/\text{Pd}(100)$ system [10]. When a molecule encounters an activated pathway the PES can lead to a change the molecule's alignment so that it is steered into a non-activated pathway. Such a mechanism would be more prevalent at low translational energies and at low rotational levels. Groß, Wilke and Scheffler's simulations showed the initial decrease in reaction probability with increased translational energy as found in experiments. They suggested that along with other degrees of freedom such as the position of the molecule on the surface, the molecule's alignment may be an important element in the steering mechanism.

Darling, Kay and Holloway also simulated dissociative reactions and found evidence of a steering mechanism [22]. They performed both classical and quantum mechanical simulations and found that anisotropies in the PES led to repositioning and re-alignment of the incoming molecule. The molecules are steered into favorable dissociative alignments, especially those in which the molecule is in the helicopter state. These steric theories predict that at certain energies, alignment of an incoming molecule may have a profound effect on its disassociation probability.

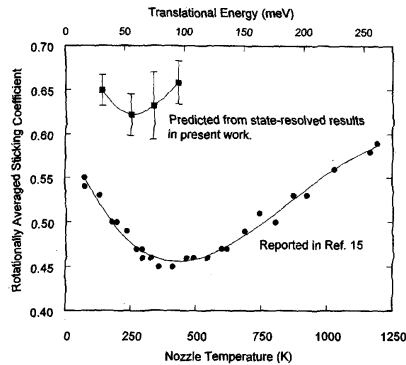


Figure 1.5: Sticking coefficient of H_2 on Pd(111) as a function of incident energy. The squares are the rotationally averaged sticking coefficient measured by Gostein and Sitz [7]. The circles were reported by Beutl et al [8]. Note that the both find the lowest sticking coefficients from 50-75 meV. Here the steric mechanism is not yet applicable and the molecules do not have enough translational energy to overcome the barriers directly.

The steering mechanism was also tested experimentally in both seeded molecular beam studies and state resolved studies [8] [7]. These studies suggest that the steering mechanism is indeed strong in the $H_2/Pd(111)$ system for energies less than about 73 meV. (See figure 1.5.) Note how the sticking coefficient reaches a minimum at around 73 meV. It is at this energy that the molecule does not have enough energy to overcome the barrier but is going too fast to be effectively steered. It is at this energy that differently aligned molecules would experience different parts of the PES without being steered into favorable pathways.

Therefore we see that the theory of steric effects predicts the experimentally verified phenomena of decreasing reaction probability with increasing energy. However, it also predicts other unexpected effects such as large anisotropies in the PES for different alignments and locations on the surface. Directly measuring these anisotropies and their relationship to the steric mechanism will be the subject for the remainder of this paper.

1.2.2 Prediction of Alignment Effects

The steric mechanism studies described above imply that there are large anisotropies in the PES that can direct a molecule to low energy pathways. If one could probe the anisotropies directly however, what could she expect to find? Let us consider only those anisotropies that have to do with the alignment of the molecule. Theorists have calculated the degree to which the alignment of the incoming molecule enhances its dissociation probability. I will discuss in some detail three such simulations from Busnengo et al., Groß and Scheffler, and Kroes and McCormack.

First, let us consider a PES calculated by Busnengo et al [9]. This work was on the $\text{H}_2/\text{Pd}(111)$ system. He asserts that the PES for Pd has a strong anisotropy with regard to molecular alignment (See figure 1.6.) From classical dynamic simulations, he study predicts that the entire translational energy dependence of the dissociation probability is due only to alignment forces at energies above 125 meV. In other words, molecules are steered toward favorable alignments rather than being steered toward favorable dissociation sites. Busnengo's work implies a strong enhancement in the dissociation probability for particular alignments; however, the dependence of the alignment effect on initial translational energy or rotational state was not discussed or explicitly calculated.

Groß and Scheffler performed a six dimensional quantum mechanical simulation and predicted that there would indeed be an enhanced probability of dissociation for helicopter molecules in the $\text{H}_2/\text{Pd}(100)$ system [10]. (This effect was also calculated on for H_2/Cu by Darling and Holloway [23].) The effect increases with increasing rotational state. The

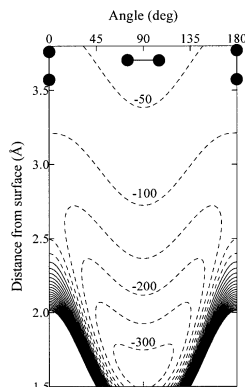


Figure 1.6: A highly anisotropic PES for the H_2/Pd system constructed by Busnengo. Molecules will be steered into favorable (helicopter) alignments by this type of PES. From Reference [9].

authors believe that this is due to molecules with high angular momentum rotating out of a favorable dissociation alignment during the dissociation event. (See figure 1.7.) The study had a fixed incident translational energy of 190 meV.

Lastly, let us consider work done by Kroes and McCormack, et al [11]. In this quantum study, the authors calculated the degree to which alignment enhancement to dissociation depended on initial translational energy. This work was done on the $\text{H}_2/\text{Cu}(100)$ system which is an activated system for all pathways. The results will certainly be different for Pd where there are many pathways with no barrier to dissociation and there is strong evidence of a steric mechanism. Still the results are the only calculations available which predict the dependence of alignment dissociation enhancement on incident translational energy. (See figure 1.8.)

In the figure it is evident that the alignment of the incoming molecule is less of a factor in the dissociation probability as the incoming translational energy decreases. There are also many details in the reaction prob-

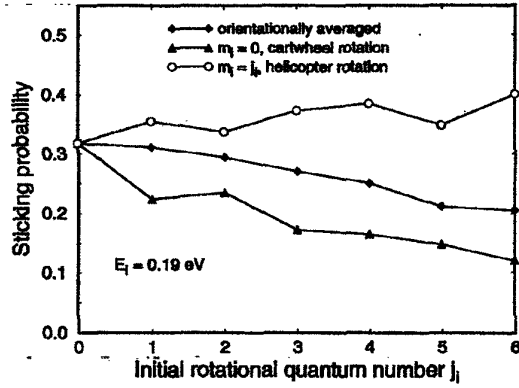


Figure 1.7: Sticking probability versus initial rotational state for different alignment distributions in the $\text{H}_2/\text{Pd}(100)$ system. The initial kinetic energy was 190 meV. Note how there is a preference for sticking for helicopter distributions. From Reference [10].

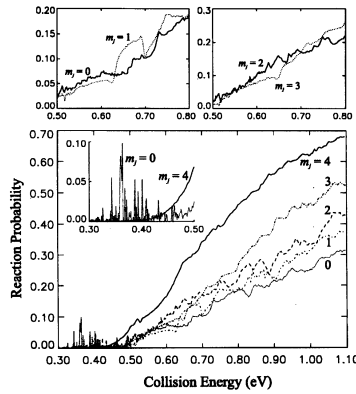


Figure 1.8: Computed reaction probabilities for the $\text{H}_2/\text{Cu}(100)$ system. Note that alignment enhancement is much more pronounced at high translational energies. Here high m_J states are helicopter molecules and low m_J states are cartwheelers. From Reference [11].

ability at low energy relating to quantum effects. Note that the lowest collision energy simulated is 300 meV, much higher than the highest energy of 72 meV tested in this study. For copper the reaction probability falls to near zero for these low energies and molecular states. For this reason we decided not to do our experiments on copper.

It is clear that there are many interesting predictions for the alignment in the molecular dissociation of H_2 on transition metals. Although the interdependence of the role alignment and incident translational energy has not been explicitly calculated for the $\text{H}_2/\text{Pd}(111)$ system, we remember from the work done by Beutl et al. and by Gostein et al. that the steric mechanism is only applicable at energies below about 73 meV. Much above 73 meV, the molecule has enough energy to overcome barriers directly. Therefore, we can expect that the alignment effect to be most important in this low energy range.

1.2.3 Previous Alignment Experiments

There has already been some experimental work on the effect of alignment on reaction probability of H_2 on transition metals. I will discuss the merits and shortcomings of each of these experiments and their results.

The first experimental evidence of an alignment effect was found in a study conducted by Gulding and Wodtke [24] [25]. This study was conducted on the (111) surface of copper and used D_2 instead of H_2 . The experiment consisted of permeating D atoms through a thin film of Cu and examining the desorbing molecules via resonantly enhanced multiphoton ionization (REMPI). Through the principle of detailed balance, the results would be comparable to that of absorbing molecules. The investigators

discovered two interesting trends. First, the polarization of the desorbing molecules was high in favor of the helicopter motion at high rotational states but the molecules were essentially randomly polarized at low rotational states ($J < 4$). This is contrary to the results predicted by Groß and Scheffler [10]. As I stated before for a Pd surface, Groß and Scheffler predicted molecular alignment at J states as low as $J = 1$. Gulding and Wodtke attribute the discrepancy to steric effects which change the alignment of the desorbing molecule as it traverses the PES toward desorption. These effects should be stronger for lower rotational states. The other possibility is that the high surface temperature (920 K) has substantially different dynamics than the simulated surface at 0 K.

The other result from Gulding and Wodtke's work is the dependence on translational energy. In permeation experiments, the corresponding incident translational energy is very difficult to determine in terms of detailed balance. However, the experimenters looked at the difference in alignment for the translational energies of desorbing molecules. Here they probed the alignment as a function of flight time. The alignment of the desorbing molecules was drastically increased at longer flight times or lower energies. This is opposite of what one might expect from a steric mechanism where slower molecules experience the anisotropic PES for a longer time and are therefore steered more into favorable alignments. Therefore, at low energies, alignment would be less important because molecules can be steered into favorable pathways. Gulding and Wodtke found the opposite trend and concluded that steric mechanisms do not play a large role in this system.

Another permeation experiment was conducted by Wetzig et al.

using both H₂[26] and D₂ [27] on Pd(100). With H₂, they found an alignment favoring the helicopter motion at all J states probed although it was statistically insignificant at J = 7. The kinetic energy of the desorbing molecules had a Maxwellian distribution with an average of 118 meV. Although, this study did not show the increase in alignment for increasing J as predicted by theory, theory and experiment agreed statistically. For D₂, Wetzig and colleagues found that there was preferential alignment for molecules in J_≥3 and J_≤7. The authors attribute the somewhat low alignment effect measured to a steering effect. But a direct probe of the effect was not available due to their inability to measure or control the molecule's translational energies.

One problem with permeation studies such as these is the inability to directly probe the relationship between alignment and translational energy in dissociation probabilities. For example in the Wetzig study, the authors can only state that their population has a Maxwellian distribution of translational energies with an average kinetic energy of 118 meV for the H₂ study. Even in the TOF studies done on copper by Wodtke and coworkers, the corresponding incident translational energy is difficult to discern[25]. In order to truly probe the effects of a steering mechanism on alignment enhanced dissociation probability one must be able to control or measure the incident translational energy and the incident rotational state. That is the goal of this study. Through molecular beam methods, we can control the average incident energies of our molecules within 2 meV. We can also look at the difference in scattering between molecules which are experiencing a steric mechanism (energies roughly <73 meV from reference [7].) and those that are not (roughly <73 meV). In this

way we should be able to directly probe the anisotropies in the PES due to alignment and their relationship to the steric mechanism.

We should also note that these types of alignment experiments have been carried out before in other systems, specifically the $\text{N}_2/\text{Ag}(111)$ system [28]. In this case, the authors were looking for the alignment of molecules which were inelastically scattered. They found that molecules in cartwheeler type alignments were much more likely to be inelastically scattered. Since we are only looking at reflection probability in this study, losses could be due to many effects including dissociation on the surface or inelastic scattering. However, the large energy mismatch between the incident energy and the energy needed to inelastically scatter H_2 into a higher rotational energy state leads to the conclusion that the most likely loss is to dissociation. This will be discussed in more detail in chapter 4.

Chapter 2

Experimental Set-Up

2.1 Apparatus

The experimental apparatus has been described previously [7, 29]. I will summarize the apparatus and detail specific changes made for the purposes of this experiment.

A schematic of the apparatus is shown in figure 2.1. A pulsed nozzle operating at 10 Hz produces a supersonic beam of H₂ molecules. The nozzle can be heated or cooled to control the translational energy and rotational distribution of the molecular beam. The pulsed molecular beam passes through a skimmer and then through a chopper which consists of a high-speed rotating disk in a differentially pumped buffer chamber. It then enters into the main chamber through a specially shaped aperture. In the main chamber, it scatters off a Pd(111) crystal at normal or near normal incidence.

The flux of the molecular beam at the sample is $\leq 1 \times 10^{12}$ /cm² per pulse or ≤ 0.00065 monolayers (ML) given the Pd(111) site density, $N_A = 1.53 \times 10^{15}$ /cm². The pulses are about 10 μ s wide temporally.

Before interacting with the surface, molecules were prepared into specific alignment states using a “pump” laser. Molecules were detected using a “probe” laser, before or after interacting with the surface depending on the relative firing time of the lasers. I will discuss the spectroscopy

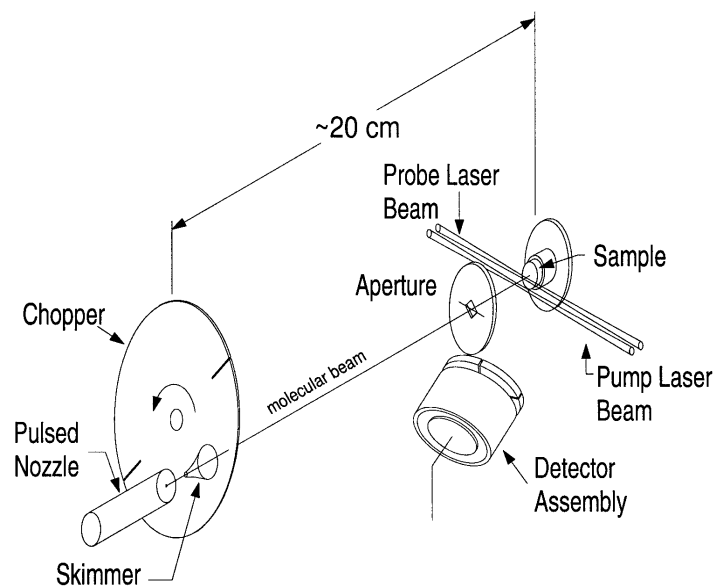


Figure 2.1: Experimental Set-up.

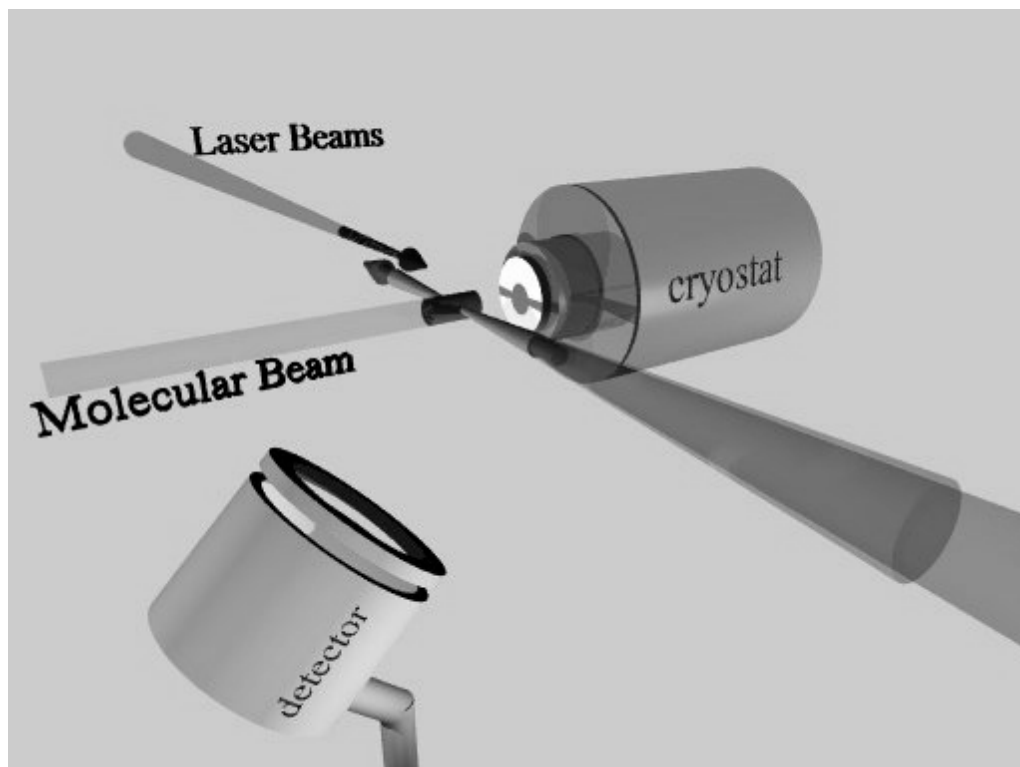


Figure 2.2: Three dimensional picture of the experimental set-up.

of both the preparation and detection in chapter 3.

2.2 State Preparation

Molecules were prepared into specific alignment states using light from a Raman process. The light was produced when the frequency doubled, circularly polarized output from a Q-switched, Nd:YAG laser was focused in a Raman cell filled with H₂ at 60 psig. A series of discrete wavelengths of light is produced by this process in accordance with Raman scattering theory. Elements in the series are shifted in energy from the incident light by integer multiples of the J=1 to J=3 energy gap in H₂. The stimulated Raman scattering for circularly polarized light is thus pure rotational ($\Delta v = 0, \Delta J = 2$) scattering. The copropagating beams exiting the Raman cell were recollimated and passed through a rotatable, linear polarizer close to the scattering chamber. The light was then focused by a 20 cm focal length lens onto the molecular beam in the chamber about 2 mm from the surface. The timing of the Q-switch was controlled so that the light intersected the pulse of the molecular beam at the highest temporal intensity. This light efficiently excited molecules from the J=1 state to the J=3 state. (More on the theory behind this transition will be discussed in chapter 3.) Since the beam waist of the laser light was significantly smaller than the spatial width of the molecular beam only a small section of the beam was excited. This produced a small amount of excited molecules that were highly localized in time and space. Typically, the temporal full width at half maximum (FWHM) of the excited molecules was 50 ns which greatly distinguished it from the thermal background which had a temporal FWHM of about 10 μ s. (See figure 2.3 The

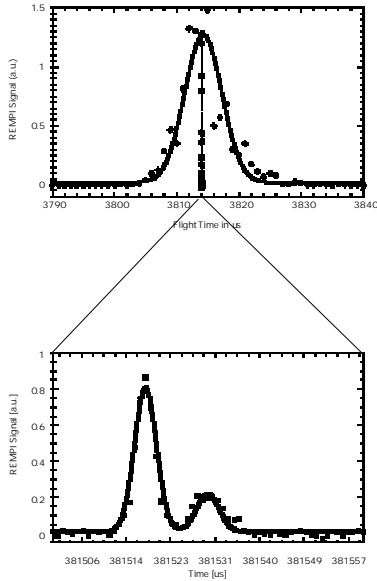


Figure 2.3: The timing of the pumped molecular pulse versus the thermal background pulse. Note how the pumped molecules are easily distinguishable from the thermal background due to the vast difference in time scales. The signal from the pumped molecules was often ten times greater than that of the thermal background.

excited molecules also had a spatial FWHM of about ~ 0.1 mm while the thermal background was at least ten times larger. Therefore, using this technique it was easy to distinguish the molecules excited into $j=3$ state via the Raman process from the thermal background.

2.3 Detection of Molecules

To detect the molecules, they were ionized using a (2+1) resonantly enhanced multi-photon ionization (REMPI) process [30, 31]. The probe laser crossed the molecular beam perpendicularly about 0.1 mm in front of the Pd sample as shown in figure 2.1. The laser can be tuned from 201 nm to 203 nm to ionize molecules in the ($v=0$, $J=3$) state via the Q branch (202.3 nm) or the S branch (201.2 nm). Ions created by the

interaction of the molecules with the laser beam are directed by steering voltages onto a microchannel plate in the bottom of the detector. The signal is amplified and recorded on a data-acquisition computer. The probe laser firing time can be adjusted with respect to the nozzle firing time and the pump laser by the computer. Scanning this time allows us to create a time of flight (TOF) measurement. A rotatable half-wave plate was available to control the polarization of the probe light. It was used in the S-branch measurements described in chapter 4.

2.4 The Pd(111) Surface

The Pd(111) sample used in this study was a disk 10 mm in diameter and 2 mm thick. It was heated from the back by electron bombardment and cooled by liquid nitrogen. The surface temperature was measured by a chromel/alumel thermocouple inserted into the crystal through a small hole spark-drilled in the side. The sample was mounted on a sample manipulator which could control the sample's height, horizontal position and the distance from the sample to the buffer chamber aperture. The lid of the main chamber could be rotated so that the sample could alternately face the molecular beam, the ion gun for cleaning or the low energy electron diffraction (LEED) or Auger Electron Spectroscopy (AES) apparatus.

2.4.1 Geometry

A quick description of the geometry of the sample is in order because corrugation is expected to play a large role in creating anisotropies in the PES with respect to molecular alignment. The (111) surface of a face-centered cubic (FCC) crystal such as Pd is remarkably flat. (See

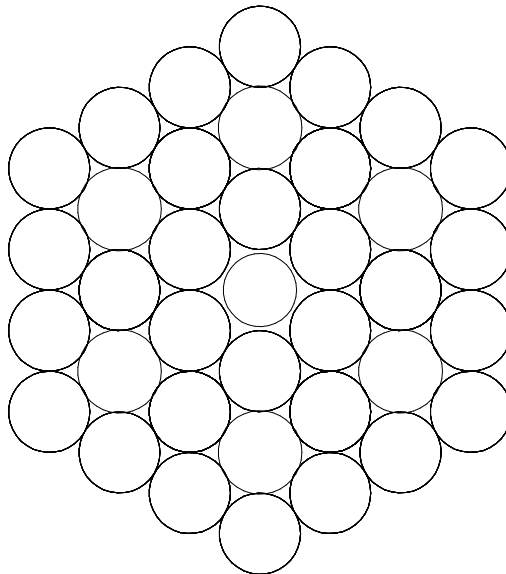


Figure 2.4: Diagram of the surface geometry of the Pd(111) surface. The surface is highly isotropic and flat.

figure 2.4.) All of the molecules on the surface are at the same height. Therefore we should expect little corrugation effect.

2.4.2 Surface Preparation

The sample was cleaned through Ar^+ ion bombardment and re-ordered through an annealing process. The following cleaning procedure was used. First, the crystal was sputtered for thirty minutes using high energy (340 eV) Ar^+ ions. The ion current was about $0.9 \mu\text{a}$. Air was used as a convenient source of oxygen to remove carbon from the surface through an oxidation process. During sputtering, the crystal temperature was held at 300°C which is above the desorption temperatures of N_2 and CO . After sputtering, the crystal was heated to 600°C for 10 minutes to anneal it and remove residual O_2 .

The order and cleanliness of the sample were checked by low energy

electron diffraction (LEED) and Auger electron spectroscopy (AES). The sample was found to be clean and well ordered. However, the presence of carbon is difficult to observe on Pd using AES. Remedies for this difficulty and experiments to further verify cleanliness are discussed in Michael Gostein's and Elizabeth Watts' dissertations [2, 32].

The sample was cleaned every two hours. It was found that after this amount of time, the intensity of the scattered signal changed. Although the base pressure of the scattering chamber was 7×10^{-10} Torr, it would rise to about 2×10^{-9} Torr with the molecular beam on.

Chapter 3

Spectroscopy

This experiment uses two types of spectroscopic techniques to prepare and detect molecules: a Raman scattering process and a REMPI process. Both of these techniques are governed by the two-photon line strength equation. I will discuss this equation in detail and explain the impact of the various terms on this experiment. Then I will show how it specifically applies to the preparation of the molecules and their detection.

3.1 The Line Strength Equation

3.1.1 The Basic Equation

The line strength equation will allow us to calculate the intensity of signal we expect for particular two-photon transitions with particular experimental geometries [1]. It is dependent on the initial and final states of the molecule as well as the geometric relationship between the polarization of the laser and the alignment of the distribution. The basic equation is:

$$I = C(det) \sum_{k,q} P_q^k(J_i, \Lambda_i, J_f, \Lambda_f; \Omega) A_q^{(k)}(J_i) n(J_i)$$

Let me explain each term in this equation. For a complete list of variables refer to table 3.1

Table 3.1: Nomenclature for the two-photon line strength equation. These are defined as in reference [1].

J_i	=	Rotational quantum number of the initial state not including nuclear spin
J_e	=	Rotational quantum number of the excited/virtual state not including nuclear spin
J_f	=	Rotational quantum number of the final/resonant state not including nuclear spin
Λ_i	=	Orbital angular momentum quantum number for the initial state
Λ_e	=	Orbital angular momentum quantum number for the excited/virtual state
Λ_f	=	Orbital angular momentum quantum number for the final/resonant state
k_a	=	Rank for the square of the first photon
k_d	=	Rank for the square of the second photon
k	=	Rank of the ground state distribution
q	=	Component of the ground state distribution
Ω	=	Angle describing the geometry of the laser beam with respect to the coordinate system describing the moments of the ground state distribution
θ	=	Angle of the laser polarization vector with respect to the lab frame
F_i	=	Total angular momentum
I	=	Nuclear spin quantum number

3.1.2 The Experimental Sensitivity Factor, $C(det)$

$C(det)$ is a detection sensitivity constant. It allows for the conversion of calculated probabilities to experimental measurements. Basically, it takes into account all of the laboratory unknowns such as the flux of laser light, the efficiency of the ion detector, the sensitivity and gain of the electron multiplier, etc.

3.1.3 The Moments of the Ground State Distribution, $A_q^{(k)}(J_i)$

The $A_q^{(k)}(J_i)$ terms describe the moments of the ground state distribution. The ground state alignment is expanded in terms of its spherical tensor components, $A_q^{(k)}(J_i)$. These moments will ultimately tell us the degree of alignment in a distribution. We are most interested in $A_0^{(2)}$, the quadrupole moment. It is the lowest order moment we can use to describe alignment. We should also note that off-diagonal elements such as $A_1^{(2)}$ describe anisotropies in the m_j state distribution. In other words, these moments will describe orientation instead of alignment. The two-photon line strength is insensitive to these anisotropies for linearly-polarized light and therefore insensitive to orientation.

The first few moments of the ground state distribution are related to the m_J states in the following manner.

$$\begin{aligned}
A_0^{(0)} &= 1 \\
A_0^{(2)}(m) &= \left\langle \frac{3m^2 - J^2}{J^2} \right\rangle \\
&= -1 + \sum_i 3P(m_i) \frac{m_i^2}{J(J+1)} \\
A_0^{(2)}(\theta) &= \frac{1}{2}(3 \cos^2 \theta - 1) \\
A_0^{(4)}(\theta) &= \frac{1}{8}(35 \cos^4 \theta - 30 \cos^2 \theta + 3)
\end{aligned}$$

Here the angle θ describes the angle between \mathbf{J} and the quantization axis, the electric field of the laser and $\cos(\theta) = \frac{m}{\sqrt{J(J+1)}}$. $P(m_i)$ is the population in each m_i state.

3.1.4 The Population of the Ground State, $n(J_i)$

The term, $n(J_i)$, is the population of the ground state. It is the total number of molecules in any state, J_i . At equilibrium, the population is determined by the Boltzmann equation:

$$n(J_i) = (2J_i + 1) \exp(-E(J_i)/kT)$$

Although nuclear spin degeneracy affects the population of each state, we will take it into account in the moments of the line strength.

3.1.5 The Moments of the Line Strength, P_q^k

The terms, $P_q^k(J_i, \Lambda_i, J_f, \Lambda_f; \Omega)$, are the moments of the line strength. They are described by the following equation:

$$\begin{aligned}
P_q^k(J_i, \Lambda_i, J_f, \Lambda_f; \Omega) &= D(q)b^k(J_i)g^k(J_i) \\
&\sum_{k_d, k_a} (-1)^k h(k_d, k_a, k, J_i, J_e, J'_e, J_f) \times \\
&\epsilon(k_d, k_a, k, q; \Omega_{lab}) \times \\
&\sum_{J_e, \Lambda_e, J'_e, \Lambda'_e} S(J_i, \Lambda_i, J_e, \Lambda_e, J_f, \Lambda_f)
\end{aligned}$$

Kummel, Sitz and Zare present a very useful derivation of the line strength in their 1986 paper [1]. This reference is a good starting point for line strength calculations. Here, I will merely summarize the contribution of each of the components of the moment of the line strength, present some calculations for the H₂ system and make some conclusions as to what each term implies in this study.

The alignment degeneracy factor, $D(q)$

This factor accounts for the symmetries one encounters when setting up such an experiment. If one defines the y axis of the experiment as the direction that the laser beam is propagating, then for a fixed k , P_q^k for a positive q is degenerate with that for a negative q . Therefore, as long as q is not zero, this factor equals two. If q is zero, $D(q = 0) = 1$.

Scaling factors for the ground state distribution, $b^k(J_i)$

These factors scale the alignment moments of the ground state distribution according to the GZ convention [33]. In this convention, $A_0^{(0)} = 1$ so that the population is independent of the ground state moments.

The angular momentum coupling terms, $h(k_a, K - d_{,k}, J_i, J - e, J'_e, J_f)$

The angular momentum coupling terms describe how the electric field of the photon couples with the angular momentum of the molecule to produce an excited state. Let us first discuss what coupling means [34]. Classically, two angular momentum vectors will add as $\vec{J} = \vec{J}_1 + \vec{J}_2$. Quantum mechanically, we have a superposition of states $|J_1 m_1, J_2 m_2\rangle$. This new state is an eigenvector of the operators, \vec{J}_1^2 , J_{1z} , \vec{J}_2^2 , and J_{2z} . The eigenvalues of J_{1z} and J_{2z} are m_1 and m_2 respectively. The state is also an eigenvector of the operators $\vec{J}^2 = (\vec{J}_1 + \vec{J}_2)^2$ and $J_z = J_{1z} + J_{2z}$. These describe a complete set of commuting operators of which $|Jm\rangle$ is the eigenvector. You can relate the superposition state, $|J_1 m_1, J_2 m_2\rangle$ to $|Jm\rangle$ through the Clebsch-Gordon coefficients by:

$$|J_1 m_1, J_2 m_2\rangle = \sum_{J, m} C(J_1 J_2 J; m_1 m_2 m) |Jm\rangle$$

For a geometric interpretation consider figure 3.1. J_1 and J_2 precess around their resultant, J . Because of this, the values for m_1 and m_2 are not well defined but the resultant projection, $m = m_1 + m_2$, is. Thus $\langle J_1 m_1, J_2 m_2 | Jm\rangle$ is the probability amplitude that at any moment $J_{1z} |Jm\rangle = m_1 |Jm\rangle$ and $J_{2z} |Jm\rangle = m_2 |Jm\rangle$.

Using this idea, we can consider how the angular momentum vectors of the photons couple with the angular momentum of the initial, excited and final states of the molecule. We can use a shorthand term for the Clebsch-Gordon coefficients called the Wigner 3-J states. Computer programs for their calculation can be found in reference [34]. The Wigner 3-J states relate how two J states, such as the initial angular momentum

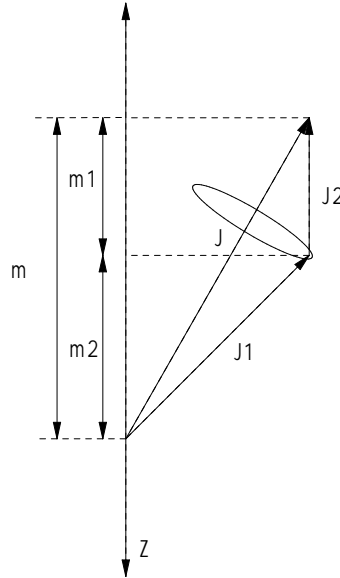


Figure 3.1: A geometric interpretation of angular momentum coupling. In the figure $\vec{J} = \vec{J}_1 + \vec{J}_2$ and $m = m_1 + m_2$. Because of the precession of \vec{J}_1 and \vec{J}_2 about \vec{J} , m_1 and m_2 are not constants of the motion.

state of the molecule and the photon couple to form a third state like the excited state. Since these coupling coefficients are dependent on the projections of the angular momentum on a space fixed axis, they depend on the moments of the ground state distribution and the moments of the photon electric field vector. I will not put the explicit form of the angular momentum coupling term here. It can be found in reference [1].

The hyperfine depolarization factor, $g^k(J_i)$

The hyperfine depolarization factor takes into account that the line strength is sensitive to \vec{J}_i instead of the total angular momentum, \vec{F} . For molecules, such as H_2 with non-zero nuclear spin, \vec{J}_i precesses in space about \vec{F} because it is coupled with the spin angular momentum, \vec{I} . \vec{J}_i may initially be aligned but a short time afterwards may become partially randomized. This effect was experimentally verified by Sitz and

Farrow [35]. Depolarization occurs for N₂ on the order of 300 ns. H₂ is an interesting case of hyperfine depolarization because only the odd J states have non-zero nuclear spin. This is due to the requirement that the total wavefunction must be anti-symmetric because the H nucleus is a fermion [36]. Symmetric rotational states, the even J states, combine with anti-symmetric spin states. In the case of H₂ with its two protons there is only one anti-symmetric spin state where I = 0. Likewise anti-symmetric rotational states, odd J states, combine with symmetric spin states. We can calculate the coupling between these states to produce the hyperfine depolarization factor via the equation:

$$g^k(J_i) = \sum_I \sum_{F_i} (2F_i + 1)^2 \left\{ \begin{matrix} F_i & F_i & k \\ J_i & J_i & I \end{matrix} \right\}^2$$

Here we have made use of the Wigner 3-j state which are directly related to the Clebsch-Gordon coefficients. We also note that the equation for $g^k(J_i)$ includes the nuclear spin degeneracy which causes a 3:1 intensity alteration for odd to even J states in H₂.

The geometric interpretation of the hyperfine depolarization factor is the same the Clebsch-Gordon coefficient geometry discussed in the previous section. (See figure 3.2.) In this case, \vec{J} is $\vec{J}1$ and \vec{I} is $\vec{J}2$. For odd J states in H₂ there are three values for the spin, \vec{I} , that couple with \vec{J} . For the even J states, I = 0 and there is no depolarization. Because of the coupling between \vec{I} and \vec{J} , m_J and m_I are not constants of the motion. So there is a time dependence to the population distribution in m_J and therefore to the alignment.

Results of a calculation of $g^k(J_i)$ are presented in figure 3.3. From the figure we see that the effect is zero for even J. The effect of hyperfine

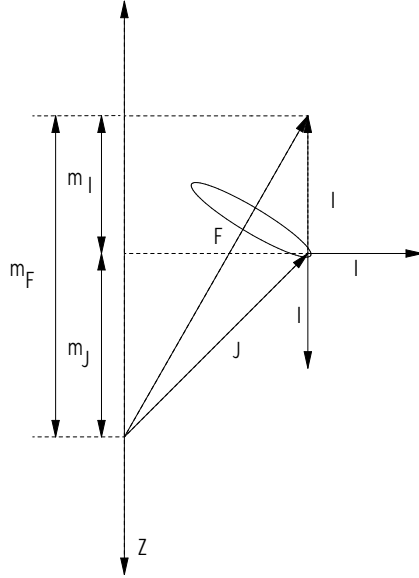


Figure 3.2: A geometric interpretation of angular momentum coupling in hyperfine depolarization. In the figure $\vec{F} = \vec{J} + \vec{I}$ and $m_F = m_J + m_I$. Because of the precession of \vec{J} and \vec{I} about \vec{F} , m_J and m_I are not constants of the motion. For odd J states of H_2 , there are two additional spin states, \vec{I} that couple with \vec{J} . For even J states, $I = 0$ and there is no depolarization.

depolarization lessens as J_i increases because the magnitude of \vec{J} increases but the magnitude of \vec{I} remains the same. Therefore as \vec{J} lengthens, there is less precession about the resultant.

The system geometry, $\epsilon(k_d, k_a, k, q; \Omega_{lab})$

This term describes the geometry of our system. A judicious choice of the lab frame vis a vis the detector frame will reduce the complexity of this factor immensely. In our experiment, the x axis is along the molecular beam. Note that this is also the surface normal. (See figure 2.1.) From this choice we see that the experiment has cylindrical symmetry. This reduces the moments of the ground state alignment to just $A_0^{(2)}$ and $A_0^{(4)}$. We can also let the lab and the detector frames coincide by defining the

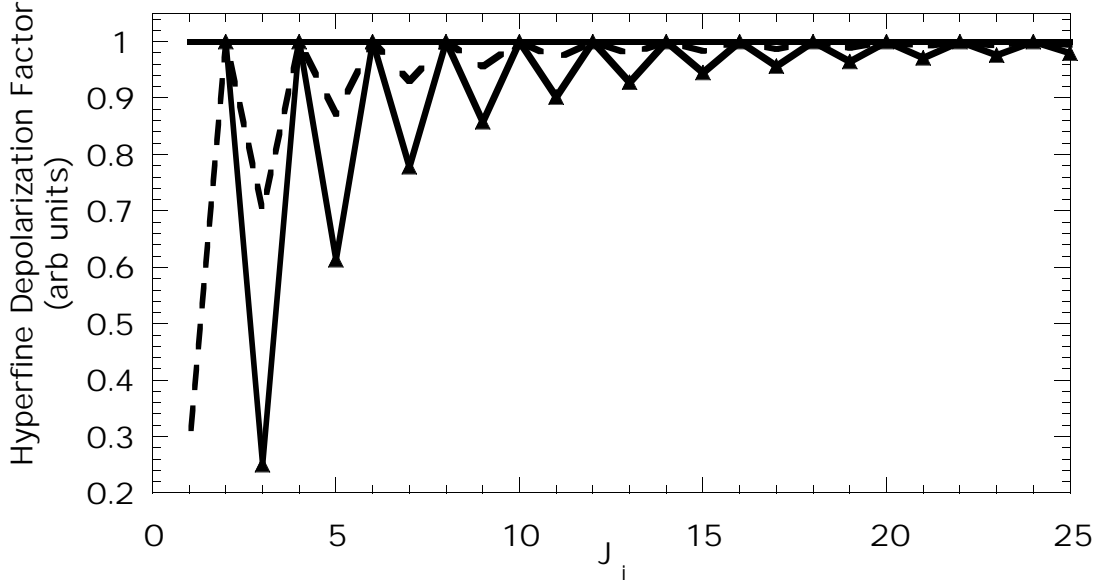


Figure 3.3: The hyperfine depolarization factor for H_2 . Shown are calculated values for P_0^0 (solid line), P_0^2 (dashed line), and P_0^4 (triangles). Note how hyperfine depolarization is less of a factor as J increases. Note also how even J 's are not depolarized because $I=0$.

z axis as the direction that the laser beam propagates. Now the angle, θ , will describe the angle between the electric field of the laser and the y axis. It will be varied in order to determine the alignment moments by changing the polarization of either the pump or the probe laser. In our experiment, the system geometry is further simplified because the first and second photons for the two-photon absorption process are identical and have the same polarization angle. ($k_a = k_d$) Therefore, the geometric factor is proportional to the spherical harmonics. Specifically:

$$\epsilon(k, q; \Omega_{lab}) \propto [(2k + 1)/4\pi]^{1/2} P_k(\cos \theta)$$

The system geometry term is the only term in the line strength equation that is dependent on the polarization of the laser. Therefore,

we can fit a variation of the detected signal with respect to the laser polarization angle to the spherical harmonics to determine the degree of alignment.

Reduced matrix elements of the dipole moment operator, $S(J_i, \Lambda_i, J_e, \Lambda_e, J_f, \Lambda_f)$

This term describes how efficiently the dipole moment operator makes transitions between states. The square of the S terms are equivalent to the Hönl-London factors. They are independent of the coupling between the photons, the coupling between the angular momentum vectors and the anisotropy of the ground state distribution. The explicit form can be calculated using Clebsh-Gordon coefficients in the form of Wigner 3 - j symbols.

$$S(J_i, \Lambda_i, J_e, \Lambda_e, J_f, \Lambda_f) = (J'_e \Lambda'_e \| r^{(1)} \| J_i \Lambda_i) * (J_e \Lambda_e \| r^{(1)} \| J_i \Lambda_i) \\ \times (J_f \Lambda_f \| r^{(1)} \| J'_e \Lambda'_e) * (J_e \Lambda_e \| r^{(1)} \| J_e \Lambda_e)$$

where

$$(J_1 \Lambda_1 \| r^{(1)} \| J_2 \Lambda_2) = (4\pi/3)^{1/2} R_{21}^{(\Lambda_2 - \Lambda_1)} (2J_2 + 1)^{1/2} \\ \times (-1)^{(J_2 - \Lambda_2)} \begin{pmatrix} J_1 & J_2 & 1 \\ \Lambda_1 & -\Lambda_2 & \Lambda_2 - \Lambda_1 \end{pmatrix}$$

and

$$(J_2 \Lambda_2 \| r^{(1)} \| J_1 \Lambda_1)^* = (-1)^{(J_2 - J_1)} (J_1 \Lambda_1 \| r^{(1)} \| J_2 \Lambda_2)$$

As one can see, the reduced matrix elements of the dipole moment operator depend on radial matrix elements, $R_{21}^{(\Lambda_2 - \Lambda_1)}$, that are generally

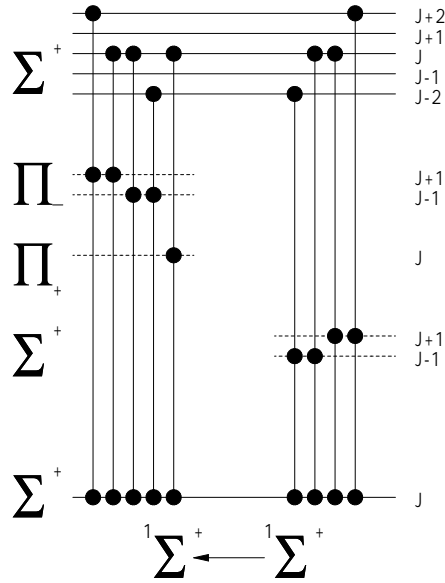


Figure 3.4: Allowed two photon transitions for $\Sigma \rightarrow \Sigma$ transitions. This figure was adapted from reference [12].

unknown. Often the radial matrix elements can be included in the detection sensitivity factor $C(det)$. Unfortunately, for H_2 , the transition involves a $\Sigma \rightarrow \Sigma$ transition in which the ratio of the transition strength of the two pathways, $\Sigma \rightarrow \Sigma \rightarrow \Sigma$ and $\Sigma \rightarrow \Pi \rightarrow \Sigma$, could make these factors unique for different pathways. The radial matrix elements can be determined empirically through a scheme outlined by Bray and Hochstrasser [12]. In this scheme, one exploits the fact that different pathways are available for different branches. Consider figure 3.4.

This figure merely shows allowed dipole transitions between states. Note how the Q branch ($\Delta J = 0$) has five pathways while the S branch ($\Delta J = 2$) has only 2. Both have pathways that are $\Sigma \rightarrow \Sigma \rightarrow \Sigma$ and $\Sigma \rightarrow \Pi \rightarrow \Sigma$. Let

$$\mu_S^2 = |2R_{ei}^0 R_{fe}^0 + 2R_{ei}^{+1} R_{fe}^{-1}|$$

and

$$\mu_I^2 = |2R_{ei}^0 R_{fe}^0 - 2R_{ei}^{+1} R_{fe}^{-1}|$$

Then the signal strength of the S branch depends only on μ_S while the Q branch depends on μ_I and μ_S . To determine the elements empirically, one measures the relative line strengths of the Q branch and S branch. From the ratio of the signal strengths, we can determine the relative ratio of the radial matrix elements. The signal strength ratio was measured, normalized for laser intensity and found to be about 10. The resulting radial matrix elements were used in the calculations.

3.2 Making an Aligned Distribution: Stimulated Raman Scattering

Now that we can calculate the intensity with which molecules make transitions through interacting with two photons, let us look at the implications of the line strength equation in preparing an aligned distribution.

Recall that, quantum mechanically, an aligned distribution is equivalent to an unequal population in the m_J states. An easy way to produce this type of distribution is to excite a molecule from one J-state to another using a two-photon transition with linearly polarized light. For this transition, selection rules insure that $\Delta m_J = 0$. Therefore, if we can promote a molecule from $J = 1$ to $J = 3$, for example, we will only populate the middle three m_J states in $J=3$ even though the m_J states in $J = 1$ were populated isotropically. (See figure 3.5.) The m_J states in the $J=3$ state will be aligned with respect to the electric field of the laser. Since in our experimental set-up, we have chosen the laser beam to be perpendicular to

the surface normal, we can create distributions which are aligned relative to the surface. Aligned distributions can be created in this manner with any J-changing transition, however we are limited because homo-nuclear diatomic molecules such as H_2 must have $\Delta J = 2$ or 0 for two photon transitions.

Since we wish to have a J-changing transition for the molecules in the chamber and we wish to pump the molecules via a Raman cell, we need to have the same J-changing transition in the Raman cell. Recall that Raman scattering will produce photons which have a difference in energy equal to the energy of the stimulated transition. (See figure 3.6.) Also, since Raman scattering is a stimulated process the strongest transition will always produce the coherent light. From the two photon line strength equation, we calculate that the Q branch transition is about 10 times stronger than the S branch transition for linearly polarized light. (We also measured this to determine the ratio of the radial matrix elements.) However, Bray and Hochstrasser show that for circularly polarized light the Q branch is much weaker than the S branch [12]. So, in order to produce a J changing transition in the Raman cell, we place a $1/4 \lambda$ waveplate in front of the cell to change the linearly polarized light produced by the YAG laser into circularly polarized light. Since we know from the Boltzmann equation that $J=1$ is the most populated state in room temperature H_2 , the S branch transition from $J=1 \rightarrow J=3$ dominates the stimulated Raman scattering.

We direct the output light of the Raman cell through a rotatable polarizer, producing linearly polarized light at a selected angle relative to the surface. We were unable to use another $1/4 \lambda$ plate to linearize

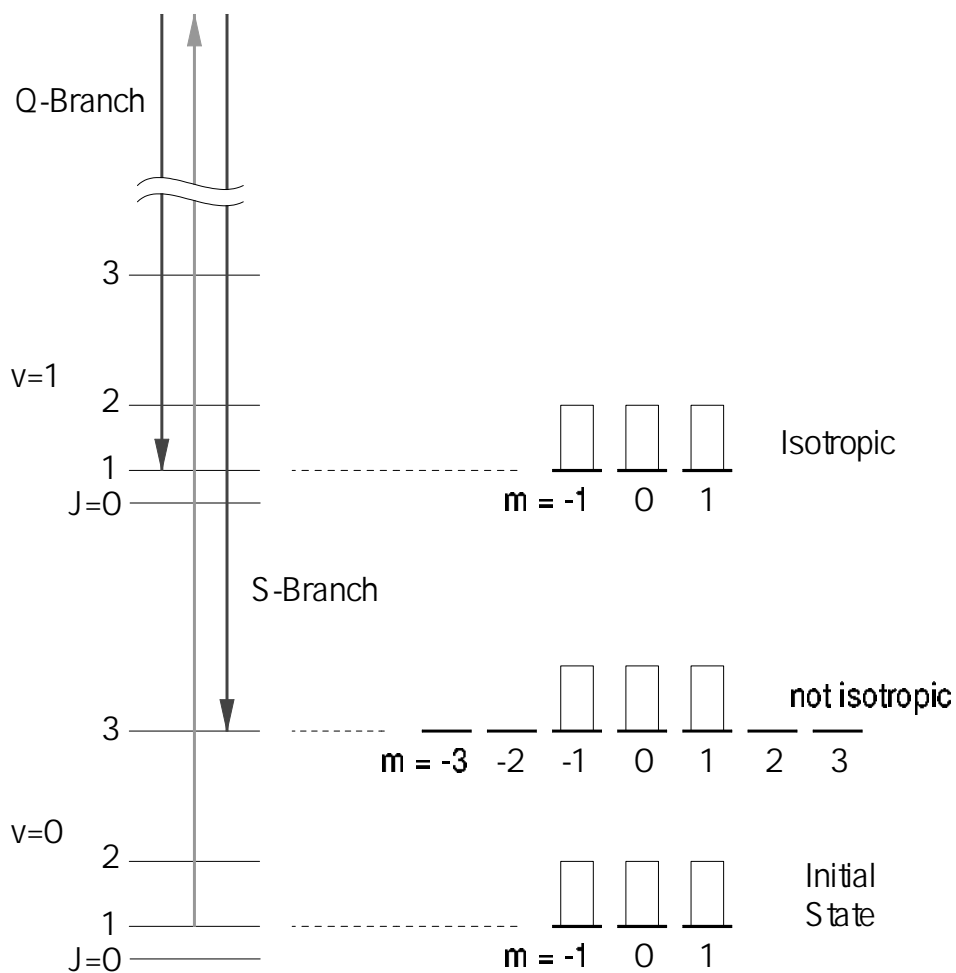


Figure 3.5: Creating an aligned distribution through an S branch transition. Molecules begin in an isotropic $J=1$ state with equal population in $m = 0, \pm 1$. As molecules are pumped to $J=3$ $\Delta m = 0$ so only the central m_J states are populated creating an aligned distribution. Molecules in $J=3$ with equal population in $m_J = 0, \pm 1$ and no population in the other m -states would have a quadrupole moment of -0.73 .

the circularly polarized light. We found that the Stokes and anti-stokes light produced by the Raman cell were of opposite helicity from the fundamental. If these were passed through a $1/4 \lambda$ plate, the anti-Stokes and Stokes light were polarized perpendicular to the fundamental. Due to conservation of angular momentum, these polarizations produced no excited molecules in the molecular beam. Therefore, we used a polarizer, which unfortunately, lessened our laser intensity by half. The polarized light is used to promote $J=1$ molecules to $J=3$ in the chamber, thus producing an aligned distribution relative to the polarization of the laser and from our choice of the lab geometry, relative to the surface.

3.3 Detecting molecules through a two-photon REMPI Process

Now that we have created an aligned distribution, we can again use the two-photon line strength equation to predict what we can expect to detect. The molecules are ionized state-selectively using (2+1) resonantly enhanced multiphoton ionization (REMPI) through the $E, F^1\Sigma_g^+ \leftarrow X^1\Sigma_g^+$ transition. (See figure 3.6.)

The degree to which the signal is modulated by the system geometry depends on the type of transition. For example, consider the calculated values for P_0^2/P_0^0 for specific values of the moments of the ground state distribution ($A_0^{(2)}$ and $A_0^{(4)}$) for the Q branch vs the S branch. (See figure 3.7.) Plotted in the figure is the expected ion intensity, normalized to the population and other branch specific factors, for different values of the relative polarization of the pump and probe lasers. So for the S branch, we expect a much larger change in measured ion intensity due to the change in the

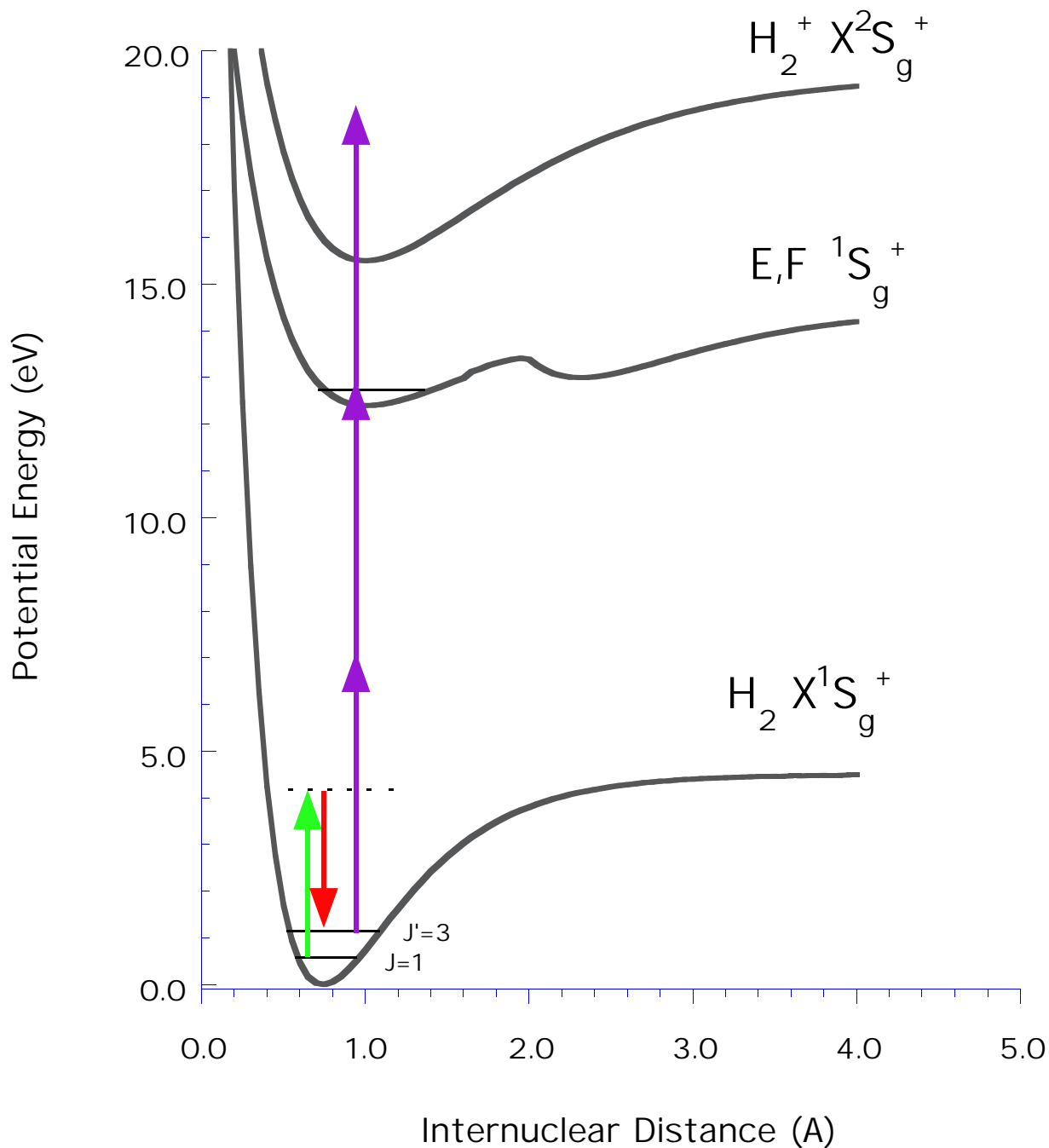


Figure 3.6: Two photon transitions involved in preparing and detecting aligned molecules in H₂. The detection of the molecules proceeds via the 2+1 REMPI process. The rotational states in the E,F ¹S_g⁺ electronic state was J=3 for the Q branch measurements and J=5 for the S branch measurements.

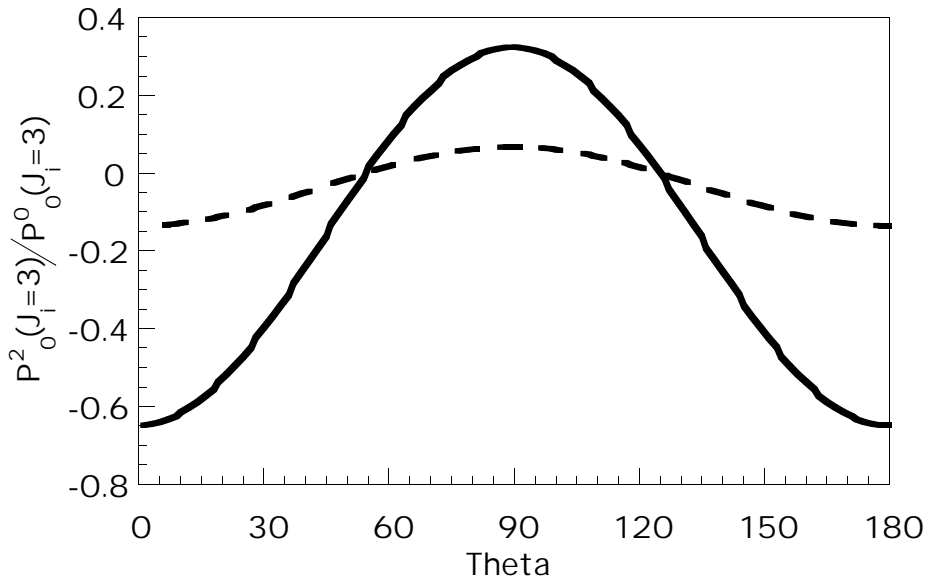


Figure 3.7: Calculated ion intensity for the quadrupole moment of the linestrength factor normalized by the population, P_0^2/P_0^0 using specific values for the moments of the ground state distribution. Here θ corresponds to the polarization of probe laser relative to the pump laser. Note the intensity changes over the range of angles much more for the S branch than for the Q branch.

relative polarization than for the Q branch.

In order to see a large change in ion intensity and therefore be better able to calculate the moments of the ground state distribution, one should use the S branch. The small change in the Q branch intensity due to the quadrupole moment would be difficult to discern especially considering the unpumped thermal background in $J=1$. However, we also know that the line strength for the S branch is ten times lower than that of the Q branch. The laser intensity in that region is also about half what it is for the Q branch. Since the ion intensity is proportional to the square of laser intensity for a two photon process, signal intensity of the S branch is less than 5 percent of that for the Q branch. The measured

relative signals are shown in figure 3.8.

Even with the large decrease in signal strength for the S branch we were able to use it to characterize the alignment of the incident beam. However, after interacting with the surface, the molecules scatter into a broad distribution and the density of the scattered signal is at most sixty percent of that of the incident even when the reflectivity is 100 percent. Also the presence of the sample tends to effect the efficiency of the ion collection and the scattered signal from the S branch was often at the limits of detectability. Because of this, we chose not to characterize the alignment of the scattered molecules using the S branch. Since we were able to characterize the alignment of the incident molecules well, we can use the Q branch to measure the reflectivity of different incident alignment distributions.

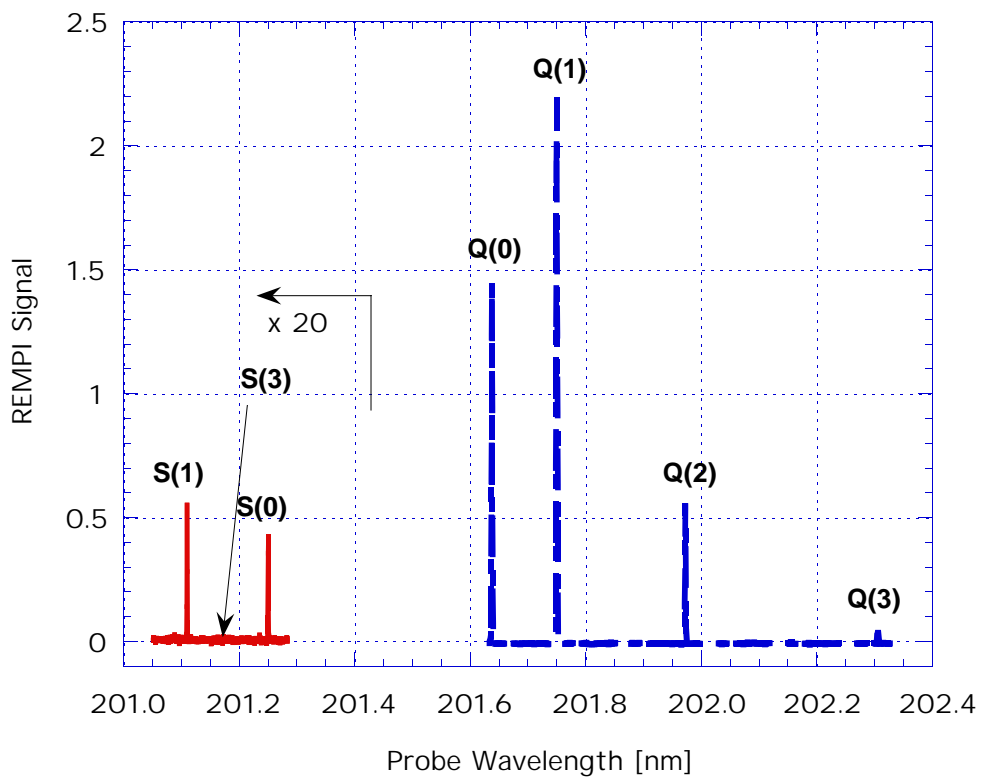


Figure 3.8: Signal strength of S vs Q branches for H_2 . The laser power at the frequency of the S branch transitions is about half of that for the Q branch transitions. The line strength for the S branch is about 10% of the Q branch line strength.

Chapter 4

Results and Conclusions

4.1 Characterization of the Aligned States

The first step in conducting this experiment was characterizing the aligned state distribution. From the framework discussed in chapter 3, we can measure the dependence of the S branch signal strength on the relative polarizations of the pump and probe lasers and extract the quadrupole moment of the ground state distribution. From this moment and our knowledge of the selection rules, we can construct an m-state distribution of the ground state. Measurements were taken of the $J=1 \rightarrow J=3$ transition while varying the polarization of the probe laser. In figure 4.2, the pump laser was polarized at 0 degrees and the probe laser waveplate was varied from 0 to ninety degrees. (We will use the following convention, a 90 degree polarization corresponds to the electric field of the laser pointing in the same direction as the surface normal. A zero degree polarization corresponds to the electric field of the laser pointing perpendicular to the surface normal.) This measurement corresponds to a distribution that has a preferential alignment of the rotational angular momentum vector perpendicular to the surface normal. Classically, the distribution consists of all cartwheelers. From the line strength equation we found that the only terms dependent on θ are the moments of the ground state distribution and the line strength. The θ dependent part of

the line strength equation can be reduced to the spherical harmonics for this geometry. Thus the theta dependent line strength equation reduces to:

$$\begin{aligned}
I(\theta) &= C(\det)\{A_0^{(0)}P_0^0 + A_0^{(2)}P_0^2\} \\
&= C(\det)\{A_0^{(0)}C_0^{(0)} + A_0^{(2)}C_0^{(2)} \times \frac{1}{2} \times (3 \cos(\theta)^2 - 1)\} \\
&= C(\det)\{1 + A_0^{(2)}\frac{C_0^{(2)}}{C_0^{(0)}} \times \frac{1}{2} \times (3 \cos(\theta)^2 - 1)\}
\end{aligned}$$

Here we have kept only the first two non-zero moments, the monopole moment and the quadrupole moment. The constants $C_0^{(0)}$ and $C_0^{(2)}$ are the part of the linestrength that is independent of θ . We set the monopole moment equal to one according to the GZ convention. We can then fit the data with the above equations to determine $A_0^{(2)}$. We can calculate the $\frac{C_0^{(2)}}{C_0^{(0)}}$ from the line strength equation developed in the previous section. This ratio is shown for different values of initial rotational state in figure 4.1.

From this analysis, we calculated quadrupole moments of vertically polarized distribution $A_0^{(2)} = -0.58 \pm .09$. This measurement was taken 0.197 μs after the interaction of the pump laser with the molecules. In a similar measurement, done at $\Delta t = 0.120 \mu\text{s}$ after the interaction, the measured quadrupole moment was higher. If only the three center m-states were populated, the quadrupole moment would be -0.73. Therefore, we see values for the quadrupole moment that are both different from what we expect and time dependent. This inconsistency in the value for the quadrupole moment could have a number of causes: an imperfect polarization of the pump laser, a spread in the angular distribution

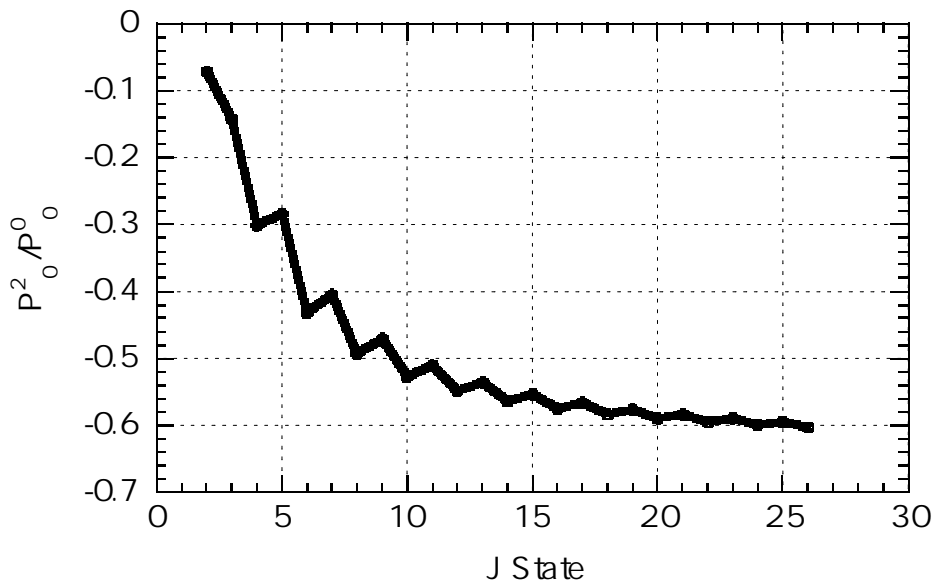


Figure 4.1: The calculated relative moments of the line strength for different values of J for the S branch in the $E,F^1\Sigma_g^+ \leftarrow X^1\Sigma_g^+$ transition in H_2 .

of the molecular beam or hyperfine depolarization. Let us consider the contribution of each cause.

If the pump polarization is not complete, the light will be elliptically polarized. This would cause m -states other than the central m -states to be populated, that is transitions other than $\Delta m = 0$ would occur. The degree of elliptical polarization would be related to the amount of population produced in the states, $m = \pm 2, \pm 3$ of $J = 3$. However, the electric field of the laser is very strong. The molecule makes many transitions between the $J = 1$ and $J = 3$ state before finally settling into the $J = 1$ or $J = 3$ state. This phenomena was tested experimentally by turning down the intensity of the laser. Even at an intensity of half of our working intensity, we still got roughly the same amount of molecules in the $J = 3$ state. Therefore, if the laser was elliptically polarized, we should expect a

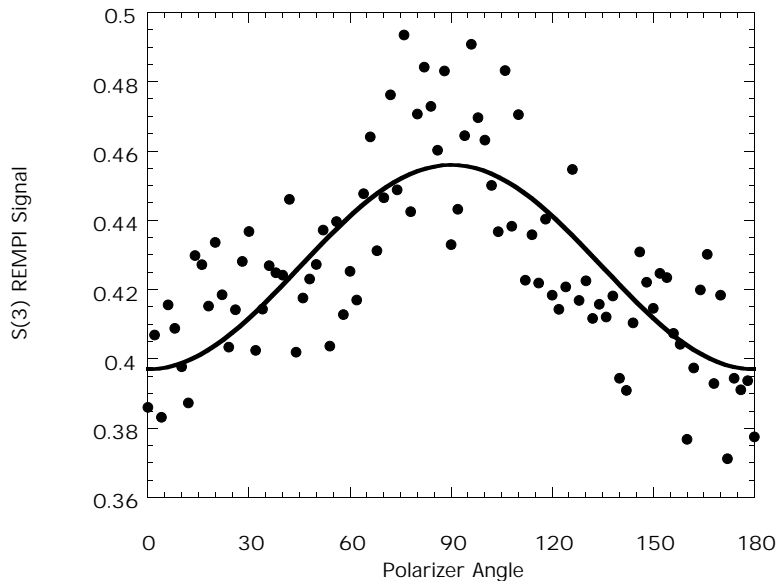


Figure 4.2: Change in ion intensity for the S(3) branch due to a change in the relative polarizations of the pump and probe lasers. In this configuration, the pump laser is polarized parallel to the surface normal.

random m-state population distribution which corresponds to a value of 0 for the quadrupole moment. Furthermore, if the effect was due to incomplete polarization we would not see the time dependence of the quadrupole moment observed.

If the molecular beam has significant spreading, the J vectors on the edge of the beam would be aligned at a different angle than those in the center of the beam. This could result in an apparent population in the outer m-states if the angle is large enough. Classically, the angle between the J vector and the quantization axis is given by:

$$\theta = \cos^{-1}\left[\frac{m}{\sqrt{J(J+1)}}\right]$$

The angles for the m-states in J=3 are given in figure 4.3. From the figure, we see that in order to apparently populate another m-state,

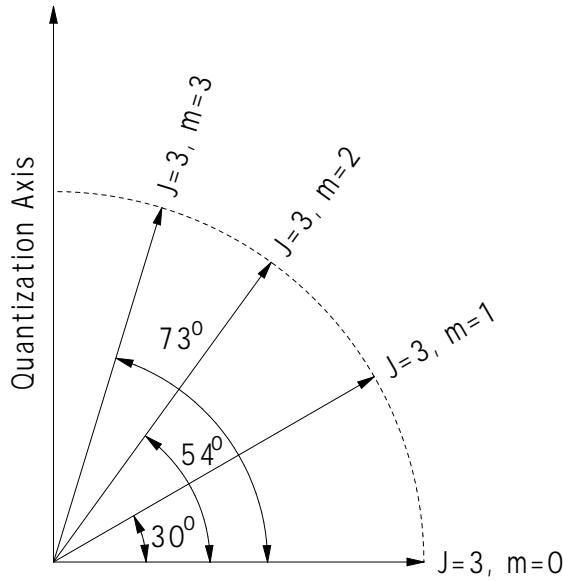


Figure 4.3: The classical representation of the angles the J vector makes with the quantization axis for different m -states.

the molecular beam spreading would have to be greater than 30° . We calculate the spreading to be no more than 1° . Therefore, the population in the outer m -states is not due to angular spreading on the molecular beam. Lastly, molecular beam spreading does not account for the time dependence of the quadrupole moment.

Lastly, let us consider hyperfine depolarization. This process is time dependent so we would expect a different contribution for the process at different time delays between the pump and the probe lasers. We should see a time dependent variation of the quadrupole moment due to the precession of \vec{J} which is coupled to the nuclear spin, \vec{I} , about the resultant total angular momentum, $\vec{F} = \vec{J} + \vec{I}$. The time dependence of the hyperfine depolarization has been measured for HF [13]. (See figure 4.4.) In the figure, one sees the quadrupole moment of HF for $J=3$ (on the left) and $J=10$ (on the right) as a function of time. The time scale of our

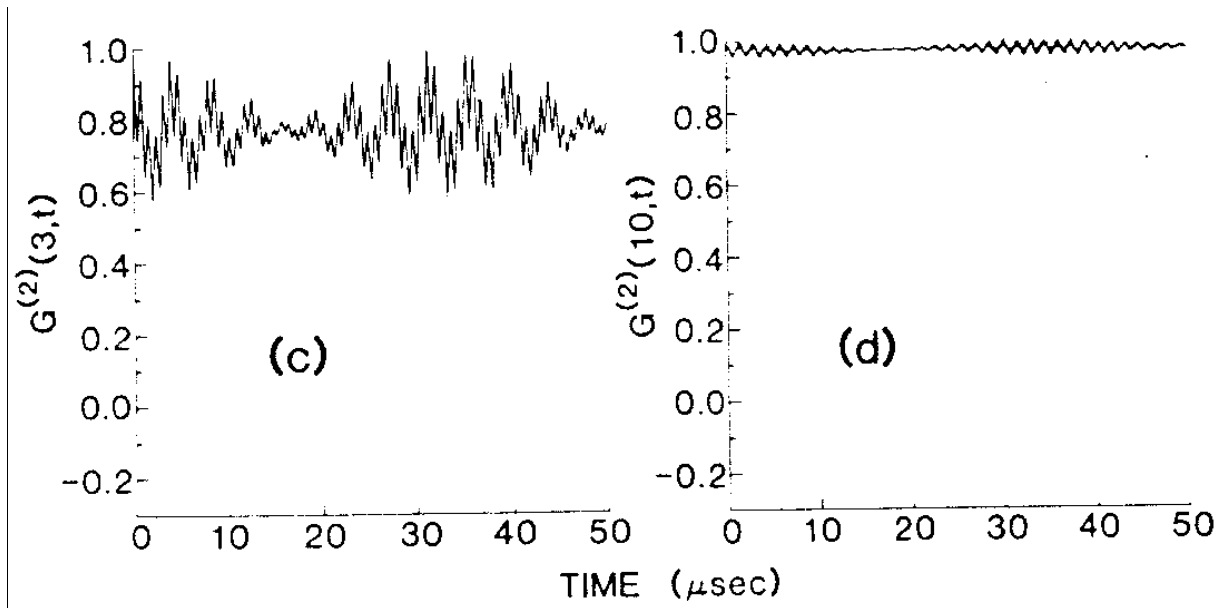


Figure 4.4: Time dependence of the quadrupole moment of HF due to hyperfine depolarization for $J=3$ and $J=10$ due to the evolution of $\vec{J} \cdot \vec{I}$. As the magnitude of J increases there is less effect. Note that in the time range of our experiment there is considerable oscillatory behavior. Taken from reference [13].

experiment is on the order of tenths of microseconds. We would be able to see the small scale structure at the beginning of the graph. Therefore, we think that the laser does align the \vec{J} with $\Delta m = 0$, but by the time we observe the quadrupole moment, it has been depolarized by its coupling with the nuclear spin.

Measurements were also taken of the S branch signal strength with respect to the polarization of the probe laser when the pump laser was polarized at zero degrees or vertically relative to the surface normal. (See figure 4.5.) Classically, this distribution consists of helicopters and cartwheelers. Its quadrupole moment was calculated as $A_0^{(2)} = -0.53 \pm .03$. Its corresponding m-state distribution will be comparable to that of the horizontal polarization case. We did not perform the change of coordinates

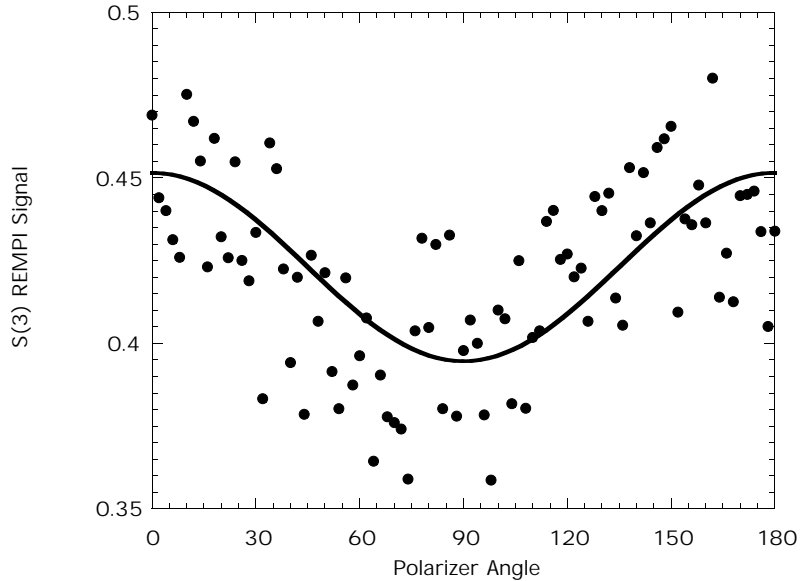


Figure 4.5: Change in ion intensity for the S(3) branch due to a change in the relative polarizations of the pump and probe lasers. In this configuration, the pump laser is polarized perpendicular to the surface normal.

necessary to put the m-state distribution for this case in the same coordinate system as the case where the pump laser is polarized horizontally. Both m-state distributions are relative to the quantization axis defined by the electric field of the pump laser.

4.2 Survival Probabilities of Aligned States

Now that we have two distinct distributions, we can see the effect of alignment on total survival probability. The first step in measuring survival probability is measuring the signal scattered from the surface. The probe laser was focused within .25 mm of the surface. The timing between the opening of chopper and the Q switch of the pump laser was optimized so that the densest part of the molecular beam was pumped. This timing was held constant for the remainder of the experiment. The

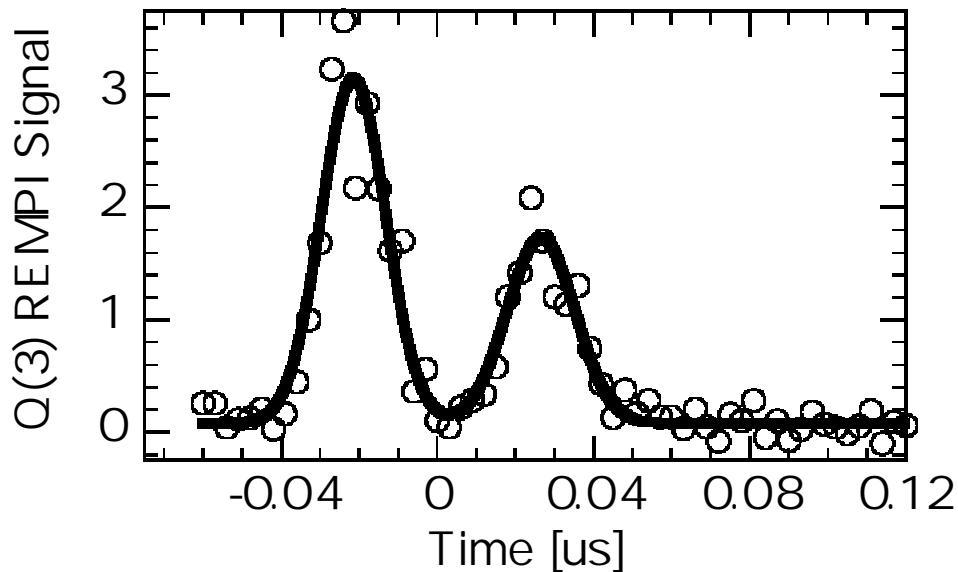


Figure 4.6: Time of flight measurement from a cold ($\sim 100K$ H_2 covered surface). The reflectivity for this type of measurement was found to be between 0.97 and 1.0 when summed over a range of scattering angles. The incident energy of this measurement was 68 meV.

relative timing between the opening of the chopper and the Q switch of the probe laser was varied so that the probe laser could temporally sample the molecular beam. The data were taken as follows: measurements are taken at a particular relative timing, the timing was adjusted, the nozzle fired again and another measurement was taken. The result of this type of measurement is called a Time of Flight (TOF). A typical TOF measurement is shown in figure 4.6. Each point in the figure represents an average of thirty shots of the nozzle at a particular relative time. Before $t=0$, the incident molecules are detected. At $t=0$ the molecules are at the surface and are out of the focus of the probe laser. After $t=0$ the molecules scattered from the surface are detected. Figure 4.6 represents a measurement done on a cold (~ 100 K) Pd(111) surface covered with H_2 and shows a high reflectivity.

It has been shown that this surface is 97-100% reflective [37]. The peak heights of the incident and scattered molecules are not equal because the molecules are scattered into a broad angular distribution while the incident molecules are more collimated. In our experiment, we are concerned with the relative survival probabilities of the two distributions rather than the absolute survival probabilities. To compute this relative survival probability, we use the area under the scattered part of the TOF curve fit to a Gaussian distribution and normalized to the area under the incident part of the TOF curve fit to a Gaussian distribution. The solid lines in figure 4.6 are Gaussian fits to the data. This method is valid as long as the two distributions (for the two pump laser polarizations) have the same scattering profile. We measured the relative signals from the two distributions at different heights of the probe laser relative to the focus of the pump laser. The heights corresponded to different scattering angles. We found little or no difference in the scattering profiles. The variation at large scattering angles is due to a very low signal to noise ratio in those data. (See figure 4.7.)

Relative survival probability measurements were taken at a surface temperature of 450 K. A typical measurement is shown in figure 4.8. In the figure we see that the area under the scattered curve for the horizontally aligned pump laser polarization (cartwheeler distribution) is greater than that of the vertically aligned pump laser polarization (helicopter/cartwheeler distribution). We repeated this measurement at a number of different incident energies. The incident energies were controlled by cooling the nozzle. Cooling the nozzle had two effects. First, it decreased incident translational energy. Second, it decreased incident

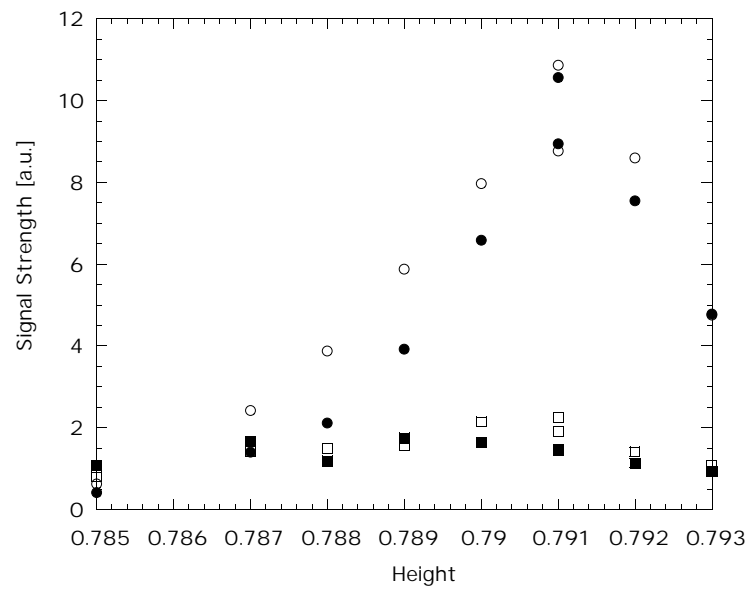


Figure 4.7: Incident and scattered beam profiles of the two distributions corresponding to different polarizations of the pump laser. In the figure, the horizontally polarized incident distribution is given by ●, the vertically polarized incident distribution is given by ○, the horizontally polarized scattered distribution is given by ■, and the vertically polarized scattered distribution is given by □.

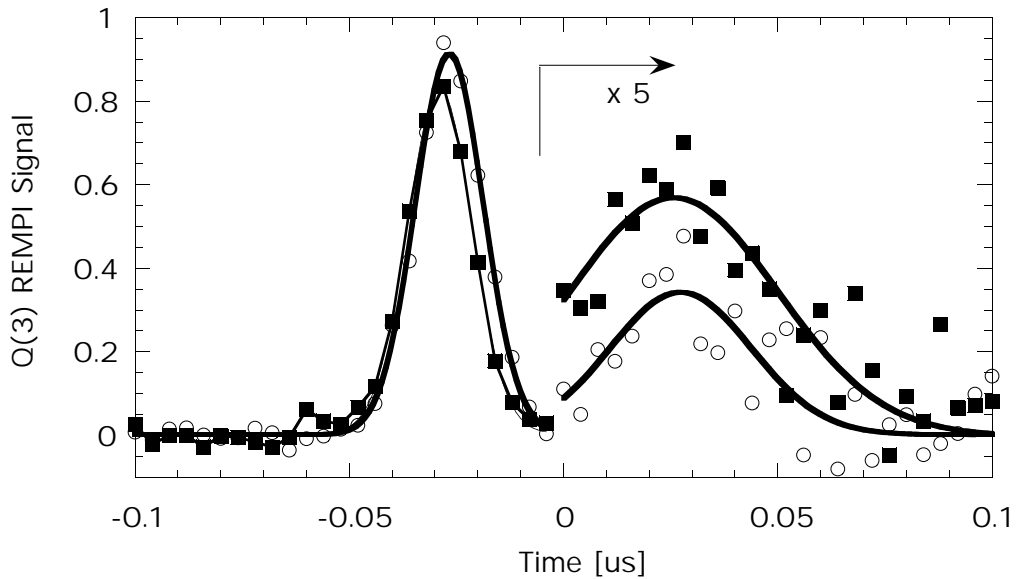


Figure 4.8: Time of flight measurement for two different polarizations of the pump laser. The horizontal polarization (■) will create a distribution that has a preference for the cartwheeler motion. The vertical polarization distribution (○) contains both helicopters and cartwheelers. The incident energy for this measurement was 64 meV. The calculated normalized ratio of the horizontal polarization distribution’s scattered signal to that of the vertical polarization was 1.53.

rotational temperature. The decrease in rotational temperature had the effect of taking population in the ground state out of $J=3$ and putting it into $J=1$. This decreased the thermal background of the experiment and increased the pumped signal strength because of the higher population in the ground state of the pump transition, $J=1 \rightarrow J=3$. In turn, the results of the cooler translational temperatures had a higher signal to noise ratio and required less averaging.

The results of the effect of translational energy on relative survival probability are shown in figure 4.9. Graphed are the ratios of the normalized area of the scattered signal of the distribution where the pump laser was polarized horizontally to that where it was polarized vertically.

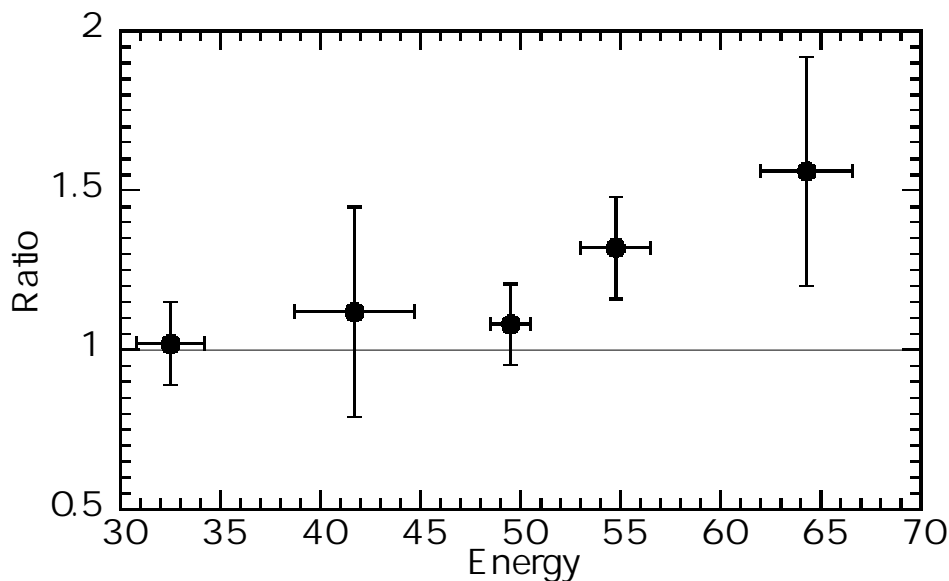


Figure 4.9: The ratio of the scattered signal from the horizontal polarization of the pump laser to that of the vertically polarized pump laser for different incident energies. Note that the ratio is highest at the energy where the steric mechanism is balanced by the ability of the molecule to overcome the barrier with incident translational energy.

A ratio of more than one indicates that the cartwheeler distribution has a greater survival probability than the helicopter/cartwheeler distribution. A ratio of one indicates that there is no preference for alignment in the survival probability.

4.3 The Stark Effect

One concern about experiments such as these is that they are reliant on the degeneracy of m_J states. If the m_J states are degenerate we can detect all of the states at a particular laser frequency. The Stark effect describes a situation where the m_J states are no longer degenerate due to a strong electric field, such as that produced by focusing a laser. This effect leads to a broadening of the line profile for a particular J *rightarrow*

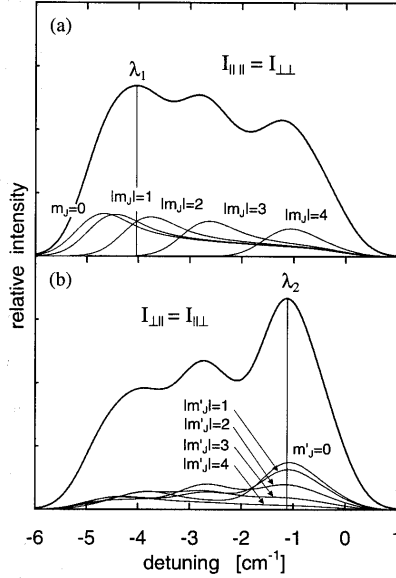


Figure 4.10: Simulated profile of the $B^1\Sigma_u^+ \leftarrow X^1\Sigma_g^+$ transition of spatially isotropic H_2 . In the simulation the maximum intensity of the Gaussian beam profile was 10 GW/cm^2 with a linewidth of $\Delta\nu = 1.0 \text{ cm}^{-1}$. The contribution of each m_J state is shown in thin lines. This figure is taken from reference [38].

J' transition. Different m_J states would contribute to the line profile at different frequencies. Wetzig et al. calculated the broadening for H_2 as shown in figure 4.10 [38].

If the m_J states are as broad in our experiment as in Wetzig's calculations, we would not be measuring all on the m_J states at any particular frequency of the probe laser. (The linewidth of the laser is only 0.07 cm^{-1} .) In order to ensure that the Stark effect was not a factor in this experiment, we measured the line profile of the Q(3) transition at different laser intensities. As shown in figure 4.11, the line profile does not change appreciably even for intensities that are 4 times greater than the least intense measurement. (Experiments were conducted at the highest laser intensity possible.) In addition to the line profile being constant, its

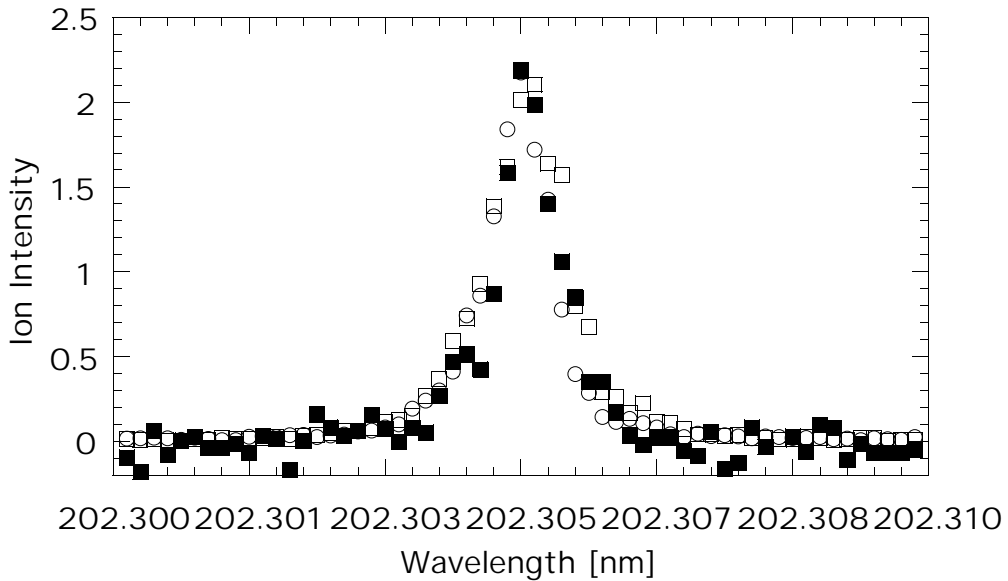


Figure 4.11: Measured linewidth at various laser intensities. The highest intensity is given by \square , 60% laser intensity is given by \circ , and 25% laser intensity is given by \blacksquare filled squares. Note how the line profile does not change with laser intensity. Each line profile can be fit with a Gaussian.

shape is Gaussian. Therefore, we do not expect any contribution from the Stark effect to change the measured m_J distribution.

4.4 Discussion

In this study, we have measured the relative survival probability of the two distributions. This does not necessarily relate directly to their dissociation probability. Survival probability measures the amount of molecules that are scattered back in their original state. Molecules can be inelastically scattered (change state) or can dissociate (not be reflected). Let us look at each of these channels and determine a likely contribution to the signal.

First let us consider inelastic scattering, specifically, rotational ex-

Table 4.1: Sticking Coefficients and Inelastic Scattering Probabilities for $J=3$. The transition probability for $J = 3 \rightarrow 5$ value is calculated from the apparent activation energy found in reference [2].

	Inc. Trans. Energy	
	55 ± 2	73 ± 3
S_3	0.47 ± 0.14	0.54 ± 0.13
$T_{3 \rightarrow 1}$	0.07 ± 0.13	0.09 ± 0.13
$T_{3 \rightarrow 5}$	0.01	

citation or relaxation. (Vibrational excitation is extremely unlikely due to the very large energy gap between the $v=0$ and $v=1$ states, 516 meV.) Because of nuclear spin statistics, H_2 is subject to the selection rule $\Delta J = \pm 2, 0$. So $J=3$ molecules could be relaxed to $J=1$ or excited to $J=5, 7$ etc. It has been shown that rotationally inelastic transitions are possible at these incident energies in this system [16, 37]. Even though the rotational spacing is larger than the incident energy the molecules are able to interact with the surface via phonons to make the transition. The important sticking coefficients and transition probabilities as measured by Gostein and Sitz [7] and Watts and Sitz [16] are given in table 4.1.

In the current experiment, the measured total loss for 67 ± 2 meV was 0.66 ± 0.1 . This value compares well with the total reflection loss expected at 73 ± 3 meV of $.63 \pm 0.18$ from the table. In fact because we had no contribution from $T_{1 \rightarrow 3}$ or $T_{5 \rightarrow 3}$ we can narrow the uncertainty in our measurement of total reflection loss. Inelastic scattering is a definite contribution to the survival probability, up to 14% for 73 meV. However, it is not the dominant mechanism. It remains to be seen if inelastic scattering is dependent upon alignment in this system as it has been seen in the

$\text{N}_2/\text{Ag}(111)$ system [28].

Since inelastic scattering will account for less than 15% of the loss, the major contribution to the survival probability is dissociative adsorption. From the data in figure 4.9, we see that the helicopter distribution is preferred over the cartwheeler distribution at incident energies in the 60 meV and up range. As the incident energy decreases, the dissociation has no preferred alignment. This is consistent with the work done by Gostein et al. [7] and Beutl [8] et al. who found that at around 70 meV, the steering mechanism is not dominant and the molecules do not have enough energy to overcome activated pathways directly. It is at this energy we should find the highest degree of alignment preference. There are no known theoretical calculations which relate alignment preference to incident translational energy for this system in the literature, therefore it is difficult to make a direct comparison to theory. However, some insight may be gained by comparing the results of Groß, Wilke and Scheffler in Figure 1.7 to our results. Recall that these data were calculated at an incident energy of 190 meV for the $\text{H}_2/\text{Pd}(100)$ system. For $J=3$, Groß et al. expect a ratio of the sticking probabilities for a pure helicopter state to a pure cartwheeler state of 2.05. Since we do not have pure states, the ratio of our helicopter/cartwheeler state to the cartwheeler state would be 1.52 according to their calculation for a mixed distribution of helicopters and cartwheelers relative to a distribution of all cartwheelers. This is not inconsistent of the value of $1.5 \pm .3$ we observe at 66 ± 3 meV. However, since the incident energies, and the distributions are different from those measured, it is still difficult to make a comparison. More work needs to be done in this area.

Chapter 5

Future Work

There are still major contributions to be made in the area of the alignment effects on dissociation on metal surfaces. Also, this experiment, with its ability to temporally isolate a single ro-vibrational state, provides an excellent opportunity to examine other areas of surface science. I will describe several attractive future projects. Determining other interesting projects in surface science is left as an exercise for the reader.

5.1 Extending the Energy Range of the Alignment Experiment

Measurements in this study were only conducted using a small range of incident energies, 32 meV to 63 meV. A larger range of energies would be interesting. At higher energies, theory predicts that the influence of alignment on dissociation probability should be less important. This is due to the molecule having enough incident translational energy to overcome the barrier directly in activated pathways. Therefore, it has less of a preference for unactivated pathways. To realize higher incident energies experimentally, one can heat the nozzle. Since hydrogen is the lightest molecule, seeding is not an option. Heating the nozzle introduces an experimental difficulty because (1) the thermal background in $J=3$ is increased and (2) the signal is lowered due to less population in the ground

state, $J=1$. This difficulty can be overcome by using a higher intensity laser, or a normalization chamber to reduce shot-to-shot noise [2].

At lower energies, theory predicts that the alignment is less of a factor in dissociation. We have already shown this trend in this study. However, we expect the ratio to become closer to unity as the translational energy is lowered. Cooler translational temperatures can be reached by seeding the gas with a heavier molecule such as nitrogen. The nozzle was already operated at near liquid nitrogen temperatures so further direct cooling would be difficult.

5.2 Alignment Effects in Other Ro-vibrational States

One of the major problems with this experiment was the hyperfine depolarization. However, if we performed the experiment using an even J state such as $J=2$, nuclear spin would be zero. Therefore, there would be no hyperfine depolarization. This would involve pumping from $J=0$ to $J=2$. Since $J=0$ has a single m -state, $m=0$, using this transition would result in perfect alignment in $J=2$ with only the central m -state populated. Any difference in the dissociation of different alignments would be enhanced due to this perfect polarization of the molecules.

There are two approaches to accomplish a $J=0 \rightarrow J=2$ pump transition experimentally. First, one could cool the Raman cell so that $J=0$ is more populated than $J=1$ and therefore dominates stimulated Raman scattering. However, since there is no mechanism for $J=1$ to transition to $J=0$ without breaking the internuclear bond, one would also need to place a catalyst in the cell to facilitate the conversion of ortho-hydrogen to

para-hydrogen. One would expect the signal strength of the measurement to be lower than that of the $J=3$ transition because the population of $J=0$ is lower than that of $J=1$ in the molecular beam. However, because the hyperfine depolarization would be zero and the molecules would occupy a single m -state, this experiment is very worthwhile.

The second approach is using a tunable laser for the Stokes light instead of a Raman cell. By using this method, one would not be reliant on the populations inside the Raman cell.

5.3 Inelastic Scattering Experiments Using the $J=3$ Temporally Isolated Signal

In previous experiments that measured the sticking coefficient of $J=3$ and its inelastic scattering probabilities, measurements were taken using a beam that had many J states occupied. Parameters were determined by changing the relative population of the J states in the incident beam, comparing them to the relative population in the scattered beam and solving a series of linear equations. In this experiment, one J state, $J=3$, is temporally isolated. Therefore, any inelastic scattering into other J states, $J=1,5,7$ etc., would be similarly temporally isolated and could only be due to the $J=3 \rightarrow J=1,5,7$ transitions. If one could measure the scattering in $J=5$ from the pumped $J=3$, one could more accurately measure that transition probability. This is very interesting especially in light of recent theoretical work done by Wang, Darling and Holloway [39] who calculate an abrupt change in the apparent inelastic activation energy for particular surface temperatures. Such a sensitive probe of the $J=3$ to $J=5$ transition, as is available in this experiment, could experimentally verify

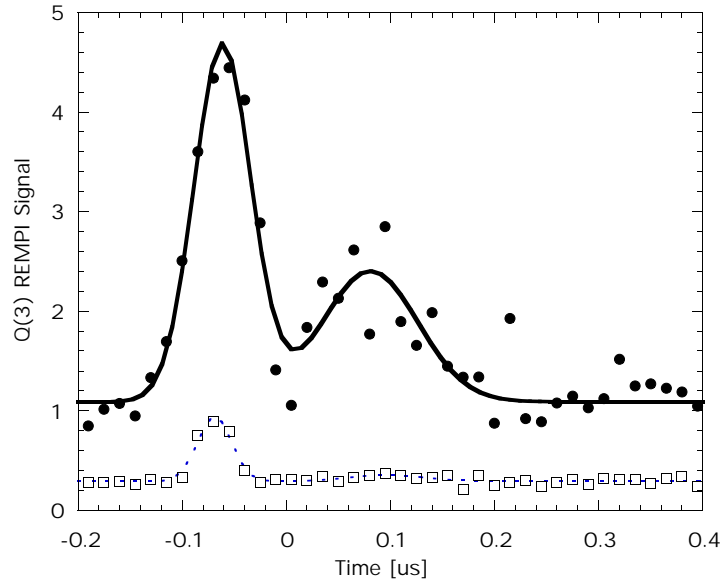


Figure 5.1: TOF measurement of $J=5$ (\square) and $J=3$ (\bullet). Note that there is some pumping into $J=5$ as evidenced by the temporally isolated $J=5$ signal that is coincident with the incident $J=3$. It is difficult to discern any $J=5$ scattering. This data was taken at an incident energy of 54 meV.

these calculations.

Preliminary measurements have been conducted in this area. It was found that at low translational temperatures, there was some $J=3 \rightarrow J=5$ transitions occurring in the Raman cell which led to an observable amount of $J=5$ in the incident beam. (See figure 5.1.) This population would make it more difficult to observe $J=3 \rightarrow J=5$ transitions in the scattered beam because there would already be some population in $J=5$ from elastic scattering. At higher translational energies, where we would expect more inelastic scattering, the scattered population in $J=5$ could not be discerned from the noise.

5.4 Measurement of the Time Development of the Hyperfine Depolarization Factor for H₂

This experiment is the perfect setup to measure the time development of the hyperfine depolarization factor for H₂. Molecules are prepared in a very small time window, .03 μ s and there is very little time spreading down stream due to the narrow translational energy. Therefore, the quadrupole moment can be measured accurately in time increments of as little as .01 μ s, merely by moving the focus of the probe laser beam with respect to the pump laser beam. For molecules moving with an average velocity of 2500 m/s, this corresponds to moving the focus downstream \sim .4 mm for each 0.1 μ s. Using this method one could accurately map out the time dependence of the quadrupole moment and therefore the evolution of $\vec{J} \cdot \vec{I}$.

Appendix

Appendix A

Alignment How-To's

Optical alignment in a two-laser, pump-probe experiment is tricky. Here I have collected some hard-earned knowledge that might be useful to future experimenters.

- The first step in this experiment is to turn on the entire experiment. Instructions on this can be found in the lab under Running Pooh.
- Tune the laser to $\text{H}_2, J=3$, dial number 24276.
- Make sure that the sample is not in place, the back lens is out, UV light is maximized through the tracking boxes and the pump laser is off or blocked.
- Align the first laser by adjusting the two steering prisms. Place an index card on the far end of the chamber to see the UV fluorescence.
- Once you can see the laser through the chamber place the aperture on a wire into the lens tube at the incident end and align by adjusting the upstream steering prism.
- Now move the aperture to the far end and align using the downstream steering prism. It is useful to use the blue glasses that block the 606 nm light to do this.

- Repeat until both ends are aligned and the blue fluorescence is in the center of the dye light.
- Put another aperture between the steering prisms and center on the UV beam. This will aid in alignment of the pump laser.
- Obtain a good signal for J=1 Q branch (at least 0.1 V for a room temperature nozzle). Note where the shadow is, where the surface is and the peak time. The time should be about $3818 \mu\text{s}$ for a chopper frequency of 300 Hz.
- Place the first lens at least .75" away from the surface when it is put in place and at least .03" above or below the shadow. Do this by adjusting the micrometers. Insure that the timing is at the maximum. Insure that the wavelength is set to maximize the signal intensity. You will now align the second lens.
- Put in the pump lens tube into the window port of the chamber.
- Close the aperture between the front two positioning prisms to almost as small as it will go.
- Align the pump lens by sliding the aperture on a wire from the front of the tube to the rear. When the aperture is in the front of the tube use the micrometers to align the vertical and horizontal positions. When the aperture is at the rear of the tube use the tilt of the tube. You can tilt the tube by slightly releasing the bolts that hold the tube onto the stand and onto the vertical positioning stage. Look to insure that the laser spot is not moving as you slide the aperture back and forth. You can use slight imperfections in the laser profile

as a guide as to whether the spot is moving as the aperture goes back and forth. IMPORTANT: Do not push the aperture all the way through the tube. The only way to get it out is to remove the tube. Then you will have to start all over again.

- Remove the tube and put on the lens. Repeat the previous exercise only this time open the front aperture a bit more. You are now looking to ensure that the UV light is in the center of the orange light. This alignment is very important or you will not get a good pumped signal.
- The distance between the pump lens and the center of the molecular beam is also important although not as critical as the rest of the alignment. This distance insures that the pump lens focuses the pumped light onto the molecular beam. The current position is the lens tube 2 11/16" from the back of the tube to the edge of the main chamber.
- Align the aperture on the pump side of the chamber to the center of the UV light.
- Now watch the orange light as it travels through the pump light optics. (The UV will be absorbed since the optics are BKT glass.) It should go through the center of the pump light aperture on the front end of the chamber. Adjust the pump steering optics so that this occurs.
- Turn on the pump laser. If you are doing alignment experiments ensure that the 1/4 waveplate is in front of the Raman cell. Steer

the pump light so that it goes through the pump aperture on the front side of the chamber. This is the same aperture you steered the residual dye light through in the previous step.

- Close the front pump aperture to about $3/4$ ". Close the back aperture to about $1/2$ " diameter and the front aperture to about $1/4$ " diameter. Align the pump light through both apertures using the two steering prisms. Ensure the light goes right through the center of each aperture. This is crucial.
- Once you are sure of your alignment open all apertures all the way.
- Now check your unpolarized pump signal. Adjust the timing on the delay generator so that the signal from the photodiode on the laser table shows the pump and probe pulses 50 ns apart. Ensure that the pump laser is firing before the probe laser. You can adjust the timing between the flash lamps and the Q switch of the pump laser by a knob on the timing box in the NIM bin. This knob will change the intensity of the pump light. In this way you can both check that the pump is before the probe and that the pump is at the highest intensity possible.
- Now insure that both the the probe light and pump light are going through the chamber, the sample is not in place, the nozzle and chopper are running and the buffer gate valve is open. You are ready to look for a signal.
- You will have to adjust both micrometers (horizontal and vertical) to find the signal. Adjusting the horizontal micrometer is the same as

adjusting the timing so you will not have to do both. It sometimes takes a long time to find the pumped signal. The most common problem leading to not being able to find the signal is misalignment.

- Once you have found the signal, it should be at or above .5V on the gated integrator sensitivity scale. You are ready to put in the polarizer in the back of the chamber.
- Close the back pump aperture to pinhole size. Put in the polarizer so that the green light is in the center of the crystal. Now open the the aperture. Check to insure the intensity of the signal is the same for both polarizations. If it is not you will have to readjust the back polarizer. Make sure that the polarizer is parallel with the back of the lens tube both horizontally and vertically. Your signal should decrease by about a factor of 2 with the polarizer in place.
- From now on you will not touch the alignment of the pump laser except to change the polarization from horizontal to vertical. (Vertical polarization is when the rejected light is exiting the polarizer and going down onto the laser table. Horizontal polarization is when the light is going to the side.) Insure that that these beams are blocked as close to the polarizer as possible.
- Now to take a TOF of the pumped signal move the b (horizontal) micrometer in front of the chamber toward the sample about .025". Changed the timing so that the start point of the TOF is the timing you used to find the signal at the overlap. Insure that the steps are $0.01 \mu s$ long.

- Some notes to help:
 - It is much easier to find the pumped signal at cold translational energies. This is because of the much higher population in $J=1$ and the lower background population in $J=3$. However, it is sometimes difficult to find the background signal at very cold nozzle temperatures.
 - When you need to cool the nozzle I found the following conversions from temperature to translational energies. These are estimated numbers and you should always measure your own translational energy. Room Temp $23^{\circ}\text{C} = 72 \text{ meV}$. $0^{\circ}\text{C} = 57 \text{ meV}$. $-32^{\circ}\text{C} = 50 \text{ meV}$. $-70^{\circ}\text{C} = 43 \text{ meV}$. $-80^{\circ}\text{C} = 32 \text{ meV}$.
 - It is sometimes difficult to find the scattered signal. It is very small for warm surface temperatures. Always look at the cold H_2 covered surface first. Then the scattered signal will be about 60% of the incident signal.

Bibliography

- [1] Andrew C. Kummel, Greg O. Sitz, and Richard N. Zare. Determination of population and alignment of the ground state using two-photon nonresonant excitation. *J. Chem. Phys.*, 85:6874–6897, 1986.
- [2] Michael Gostein. *Quantum State Resolved Studies of Elastic and Inelastic Scattering of H₂ from Cu and Pd*. PhD thesis, The University of Texas at Austin, 1999.
- [3] G. J. Kroes, E. J. Baerends, and R. C. Mowrey. Six-dimensional quantum dynamics of dissociative chemisorption of H₂ on Cu(100). *J. Chem. Phys.*, 107:3309–3323, 1997.
- [4] Axel Gross. Reactions at surfaces studied by *ab initio* dynamics calculations. *Surface Science Reports*, 32:291–340, 1998.
- [5] S. Wilke and M. Scheffler. The coadsorption of H₂ and S on pd(100). *Surf. Sci.*, 329:L605, 1995.
- [6] S. Wilke and M. Scheffler. Potential-energy surface for H₂ dissociation over Pd(100). *Phys. Rev. B*, 53:4926–, 1996.
- [7] M. Gostein and G. O. Sitz. Rotational state-resolved sticking coefficients for H₂ on Pd(111): Testing dynamical steering in dissociative adsorption. *J. Chem. Phys.*, 106:7378–7390, 1997.

- [8] Michael Beutl, Manfred Riedler, and Klaus D. Rendulic. Strong rotational effects in the adsorption dynamics of $\text{H}_2/\text{Pd}(111)$: evidence for dynamical steering. *Chem. Phys. Lett.*, 247:249–252, 1995.
- [9] H.F. Busnengo, C. Crespos, W. Dong, A. Salin, and J.C. Rayez. The role of orientational forces in non-activated molecular dissociation on a metal surface. Private communication, 2000.
- [10] Axel Gross, Steffen Wilke, and Matthias Scheffler. Six-dimensional quantum dynamics of adsorption and desorption of H_2 at $\text{Pd}(100)$: Steering and steric effects. *Phys. Rev. Lett.*, 75:2718–2721, 1995.
- [11] Drew A. McCormack, Geert-Jan Kroes, Roar A. Olsen, Evert-Jan Baerands, and Richard Mowrey. Rotational effect in six-dimensional quantum dynamics for reaction of H_2 on $\text{Cu}(100)$. *J. Chem. Phys.*, 110(14):7008–7020, 1999.
- [12] R.G. Bray and R.M. Hochstrasser. Two-photon absorption by rotating diatomic molecules. *Molecular Physics*, 31:1199–1211, 1976.
- [13] Robert Altkorn, Richard Zare, and Chris Greene. Depolarization of optically prepared molecules by two randomly polarized spins. *Molecular Physics*, 55:1–9, 1985.
- [14] J. E. Lennard-Jones. *Trans. Faraday Soc.*, 28:333, 1932.
- [15] G.P. Brivio and M.I. Trioni. The adiabatic molecule-metal surface interaction: Theoretical approaches. *Reviews of Modern Physics*, 71:231–265, 1999.

- [16] E. Watts and G. O. Sitz. Surface temperature dependence of rotational excitation of H_2 scattered from Pd(111). *J. Chem. Phys.*, 111:9791–9796, 1999.
- [17] Elizabeth Watts, G.O. Sitz, D. A. McCormack, G. J. Kroes, R. A. Olsen, J. A. Groeneveld, J. N. P. Van Stralen, E. J. Baerends, and R. C. Mowrey. Rovibrationally inelastic scattering of H_2 ($v=1, J=1$) from Cu(100): Experiment and theory. *J. Chem. Phys.*, 114:495–503, 2001.
- [18] H. F. Busnengo, W. Dong, P. Sautet, and A. Salin. Surface temperature dependence of rotational excitation of H_2 scattered from Pd(111). *Phys. Rev. Lett.*, 87:1276011–1276014, 2001.
- [19] K. D. Rendulic, G. Anger, and A. Winkler. Wide range nozzle beam adsorption data for the systems H_2 /Nickel and H_2 /Pd(100). *Surf. Sci.*, 208:404–424, 1989.
- [20] Ch. Resch, H.F. Berger, K.D. Rendulic, and E Bertel. *Surf. Sci.*, 316:L1105, 1994.
- [21] K.D. Rendulic and A. Winkler. *Surf. Sci.*, 299/300:261, 1994.
- [22] G. R. Darling, M. Kay, and S. Holloway. The steering of molecules in simple dissociation reactions. *Surf. Sci.*, 400:314–28, 1998.
- [23] G. R. Darling and S. Holloway. Rotational motion and the dissociative of H_2 on Cu(111). *J. Chem. Phys.*, 101:3268–3281, 1994.
- [24] S. J. Gulding, A. M. Wodtke, H. Hou, C. T. Rettner, H. A. Michelsen, and D. J. Auerbach. Alignment of $\text{D}_2(v,J)$ desorbed from Cu(111):

- Low sensitivity of activated dissociative chemisorption to approach geometry. *J. Chem. Phys.*, 105:9702–9705, 1996.
- [25] S. J. Gulding, A. M. Wodtke, H. Hou, C. T. Rettner, H. A. Michelsen, and D. J. Auerbach. Alignment of $D_2(v,J)$ desorbed from Cu(111): Low sensitivity of activated dissociative chemisorption to approach geometry. *Science*, 277:80–82, 1997.
- [26] D. Wetzig, M. Rutkowski, W. Etterich, R. David, and H. Zacharias. Rotational alignment in associative desorption of H_2 from Pd(111). *Surf. Sci.*, 402-404:232–235, 1998.
- [27] D. Wetzig, R. Dopheide, M. Rutkowski, R. David, and H. Zacharias. Rotational alignment in associative desorption of D_2 from Pd(111). *Phys. Rev. Lett.*, 376:463–466, 1996.
- [28] G. O. Sitz, A. C. Kummel, and R. N. Zare. Direct inelastic scattering of N_2 from Ag(111). I. Rotational populations and alignment. *J. Chem. Phys.*, 89:2558–2571, 1988.
- [29] Jennifer L. W. Siders and Greg O. Sitz. Observation and characterization of direct inelastic and trapping desorption channels in the scattering of N_2 from Cu(110). *J. Chem. Phys.*, 101:6264–6270, 1994.
- [30] E. E. Marinero, C. T. Rettner, and R. N. Zare. Quantum-state-specific detection of molecular hydrogen by three-photon ionization. *Phys. Rev. Lett.*, 48:1323–1326, 1982.
- [31] E. E. Marinero, R. Vasudev, and R. N. Zare.

- [32] Michael Gostein. *Dynamical Effects in Dissociative Adsorption: Quantum State-Resolved Studies of H₂ Scattering from Pd and Cu*. PhD thesis, The University of Texas at Austin, 1997.
- [33] C.H. Greene and R.N. Zare. Determination of product population and alignment using laser-induced fluorescence. *J. Chem. Phys.*, 78:6741, 1983.
- [34] R. N. Zare. *Angular Momentum, Understanding Spatial Aspects in Chemistry and Physics*. Wiley, New York, 1988.
- [35] G. O. Sitz and R. L. Farrow. Preparation and decay of alignment in N₂(v=1). *J. Chem. Phys.*, 101:4682–4687, 1994.
- [36] J. I. Steinfeld. *Molecules and Radiation: An Introduction to Modern Molecular Spectroscopy*, chapter 4. The MIT Press, 1978.
- [37] M. Gostein, E. Watts, and G. O. Sitz. Vibrational relaxation of H₂ on Pd(111). *Phys. Rev. Lett.*, 79:2891–2894, 1997.
- [38] D. Wetzig, A.D. Rudert, and H. Zacharias. Measurement of the rotational alignment in the presence of the second order stark effect. *Eur. Phys. J. D*, 17:181–188, 2001.
- [39] Z. S. Wang, G. R. Darling, and S. Holloway. Surface temperature dependence of the inelastic scattering of hydrogen molecules from metal surfaces. *Phys. Rev. Lett.*, 87:1–4, 2001.

Vita

Marcia Joyce Isakson nee Geiger was born on January 29, 1970 to Edwin and Joyce Geiger from Oak Forest, Illinois. She attended New Milford High School from which she graduated as salutatorian in 1988. She then went on to attend the United States Military Academy at West Point, New York. She graduated in 1992 receiving honors for the highest academic record in physics and the natural sciences. After graduation, Marcia accepted a Hertz Foundation Fellowship for the study of atomic and molecular physics. She attended the University of Texas at Austin and received a master's degree in 1994 for her work studying the chemical reactions involved in the destruction of the ozone layer. She then attended the Ordnance Officer's Basic Course at Aberdeen Proving Grounds Maryland, graduating first in her class. Marcia went on to serve in the United States Army in the 554th Maintenance Battalion as a warehouse officer, maintenance shop officer and battalion operations officer. She left the army as a captain in 1997 and resumed her work at the University of Texas under the direction of Dr. Greg Sitz studying the dynamics of gas-surface reactions. She married John (Ike) Isakson in 1992. They have two children, Grace and Nicholas.

Permanent address: 1501 Tamar Lane
Austin, Texas 78727

This dissertation was typeset with L^AT_EX[†] by the author.

[†]L^AT_EX is a document preparation system developed by Leslie Lamport as a special version of Donald Knuth's T_EX Program.